63-1-5

FORWARDED BY THE CHIEF, BUREAU OF SHIPS

[redacted]

HUGHES TOOL COMPANY · AIRCRAFT DIVISION
Culver City, California

Report HTC-62-42

HYDROSTREAK WATER SCOOP STUDY

FINAL REPORT

July 1962

Prepared Under U. S. Navy, Bureau of Ships
Contract NObs-4329 (Index No. SF-0130207)

Prepared by: N. B. Hirsh
N. B. Hirsh
Supervisor - Hydrodynamics Laboratory

R. W. McJones
R. W. McJones
Consultant - Hydrodynamics

Approved by: H. O. Nay
H. O. Nay
Manager, Technical Department

HUGHES TOOL COMPANY -- AIRCRAFT DIVISION
Culver City, California

TABLE OF CONTENTS

LIST OF ILLUSTRATIONS

1. ABSTRACT

A new vertical free-jet hydrodynamic test facility is checked out during a series of tests of ram inlets, fully submerged bodies and discs, surface piercing struts, and low aspect ratio planing models. Test conditions include Froude number of infinity, cavitation number of zero, and Reynolds Number of 1.5×10^6. Excellent agreement is found with available results from the literature wherever comparison is possible. Cambered and flat planing surfaces of several plan forms are tested from initial water contact through full wetting to deep submergence. Lift drag ratios near 10 are found in several cases. A complete water scoop configuration is established for high speed overwater vehicle application and its lift, drag, and pressure recovery fully validate the scoop performance assumptions incorporated into previous Hydrostreak performance estimates.

2. INTRODUCTION

Work under the subject contractual agreement represents one phase of a continuing program by the Bureau of Ships and the Hughes Tool Company - Aircraft Division to define the ultimate operational characteristics of ground effect machines in general and of Hydrostreak vehicles in particular.

The Hydrostreak vehicle concept is based on the containment of a compressed air bubble by a thin curtain of water. Since its inception in 1959 this system has been the subject of a research effort by this contractor under Bu-Ships Contracts NObs 4329, 4337 and 4400. Initial analysis pointed out the inherent performance advantages over all-air systems and pinpointed the areas requiring additional research effort. The Hughes Hydrodynamics Laboratory was established to study water curtain containment of compressed air and succeeded in documenting useable configurations. Two prototype vehicles were built and tested to demonstrate the over-all feasibility of the system and to explore dynamics and performance problems.

The design of water scoops for high speed vehicles posed questions not answered in the available literature and led to the present program. In the course of modifying the Hughes Laboratory for the present work, it became apparent that this research could be of general value over and above its application to the Hydrostreak vehicle. Accordingly, both the test program and this report have been slanted toward the secondary goal of contributing to the general field of high speed hydrodynamics.

The model parameters to be varied and the range of variables to be considered were established in coordination with the Bureau of Ships Project Office. Results of early tests were used to modify and refine the models and test procedures. A full scale model design, based on test results, is included in this report.

3. NOMENCLATURE

A	Cross - Sectional Area - square inches
A_i	Inlet Area - square inches
AR	Aspect Ratio
b	Beam Width of Planing Models (for circular discs and ellipse $b = \sqrt{S}$) - inches
c	Chord - inches
C_{DA_i}	Drag Coefficient Based on Inlet Area
C_{D_π}	Drag Coefficient Based on Projected Frontal Area
C_L	Lift Coefficient
d	Depth of Immersion (measured from point of initial model contact)- inches
D	Drag - lbs.
D_o	Inlet Momentum Drag - lbs.
F_h	Froude Number Based on Depth of Immersion
Δ H	Head Loss - inches Hg or psi
L	Lift - lbs.
P	Pressure - inches Hg or psi
Δ P	Differential Pressure - Inches Hg or psi
q_o	Free Stream Dynamic Pressure - inches Hg or psi
Q	Volume Flow Rate - cfm
R	Inlet Radius (w/2 for square inlets) - inches

RN	Reynolds Number
S	Plan Form Area - square inches
V_i	Inlet Velocity - fps
V_o	Free Stream Velocity - fps
V_i/V_o	Inlet Velocity Ratio (mass flow ratio)
w	Width - inches
β	Conical Angle - degrees
ρ	Density - slugs per ft^3
σ	Cavitation Number
τ	Angle of Attack (trim angle) - degrees
r	Lip Radius - inches
r/R	Lip Roundness Ratio

4. EQUIPMENT AND TEST PROCEDURE

The Hughes Hydrodynamics Laboratory was originally established for testing of water curtains suitable for retaining the lifting air bubble under Hydrostreak type vehicles. The Laboratory contains a 50 HP main pump capable of supplying a 5.0 inch diameter free jet of water at 30 fps.

The laboratory has been modified for the present program to the configuration shown in Figure 1. A stilling chamber assembly with a volume of approximately 11 cubic feet and a 6.25 inch diameter discharge orifice is connected to the main pump discharge. Various layers of flow straightener are employed to provide a stable and smooth free jet (see Figure 2). A pitot traverse check of the free jet shows negligible variation in dynamic pressure across the stream. The cavitation bubble seen in Figure 8 will illustrate the lack of turbulence in the free jet.

Flow from the vertical free jet enters the 2350 gallon storage tank. The supply pump removes 1800 gallons per minute from the tank at the maximum pumping rate. The small size of the supply tank, with respect to the water flow rate, originally caused problems of air entrainment. The addition of baffles to the storage tank eliminated this problem.

A flow splitter assembly is utilized to scoop off one side of the stream to produce a flat water surface. It was found that one sharp edged blade would not produce a smooth surface; however, a cascade effect utilizing two staggered

sharp edged blades placed at a slight angle to the stream, produces a relatively flat and smooth water surface (see Figures 13 and 16).

A combination force measurement and internal flow system is used. This system is shown in Figure 3. Loads exerted by the models in the "x" and "y" directions (lift and drag respectively) are transferred through the hollow model support beam to the hollow load cell. The system is designed so that loads are nominally exerted at the center line of the load cell and at a known distance along the "z" axis from the cell (see Figure 4). Due to symmetry of the models, the "z" distance is constant for all testing. Calibration data indicate negligible torque sensitivity to eccentric loading along the "x" and "y" axis and no interaction between lift and drag loads.

Internal flow from the models is ducted through the model support beam, the load cell, the diffuser section and the discharge hose to the 15 HP auxiliary pump. The pump discharges through a 1.50 inch diameter pipe to a flow measuring section consisting of a 1.00 inch diameter square edged orifice plate with flange taps. The water is then returned to the supply tank. Two throttling valves in the pump discharge pipe provide close control of the model inlet flow.

The model support assembly is mounted to a rotary table with the capability of locating the models at any point in the stream. Angle of attack and depth of immersion can be continuously varied during model testing to closely controlled locations.

Instrumentation consists of a strain indicator, a differential manometer connected to the flow measuring orifice and a ten tube manometer utilized for various model pressure taps. During the course of the test program the strain indicator drag and lift load conversion factors remained constant within $\pm$ 2%. Zero return of the instrument was within the same margin.

Tests were conducted at a free stream dynamic pressure of 6.0 inch Hg and 10.0 inch Hg. Reynolds Numbers for these conditions are $.205 \times 10^6$ per inch of model and $.265 \times 10^6$ per inch of model, respectively. The Froude number for a 6 inch long model moving at a velocity of 30 fps in a horizontal direction is 7.5, which is beyond the critical region below $F \approx 3.0$; however, under conditions of vertical flow, where there is no restoring force, the Froude number approaches infinity.

Because of the vertical operating position of the models, the dynamic pressure increases downward along the model in an amount equal to the static head difference. For the longest model tested (6.67 inches) the dynamic pressure increases in the order of 5% from the leading edge to the trailing edge of the model. For purposes of data reduction, the dynamic pressure is determined at the leading edge of the model except in the case of planing models, where it is determined at the trailing edge of the model.

The model test program employs the models shown in Figure 5. Models are of six basic types consisting of a thin wall inlet, drag discs, drag bodies, inlet model, planing models and a final model. For model geometry see Figure 24.

The thin wall inlet has been tested in both a sharp edged and rounded lip configuration. A non-metric shield is used to isolate all but the upper .50 inch of the inlet pipe from the water flow. Care is taken to prevent impingement of spray on the lower portion of the inlet and to prevent any water flow between the model and the shield. Therefore, a very negligible portion of the drag load can be attributed to skin friction. Tests have been conducted at two dynamic pressures and various inlet mass flow ratios.

The thin wall inlet is used to support the drag discs, the drag bodies and the inlet model. The non-metric shield is installed during these tests. A series of drag discs has been evaluated at various dynamic pressures. Three bodies of revolution (cone, paraboloid and ellipsoid) are used for drag body testing at various dynamic pressures. The inlet model is a modified version of the ellipsoidal drag body. Tests include two dynamic pressure conditions at various inlet mass flow ratios. The inlet lip has been varied to determine the optimum shape.

During the tests of drag discs, drag bodies and the inlet model, a capability was added to the system to both sense bubble pressure and to add air to the bubble. However, results during artificial ventilation of the bubble were inconsistent and revisions were made to permit a greater degree of natural ventilation. With the added natural ventilation, cavitation numbers of less than .001 are obtained. All results are shown in the naturally ventilated condition.

The planing models are mounted on a strut supported from the model support beam. A flat rectangular plate, a flat disc, a cambered disc and a flat elliptical plate have been tested at varying immersions and at varying angles of attack. The ellipse also has been tested operating as a high aspect ratio ski and in a cambered configuration.

Three circular cylinders and three blunt based struts (wedge, ogive and ellipse) have been tested at various immersions. Angle of attack and angle of yaw variations have not been attempted.

The final model has been tested with and without a ski at various immersions for a constant inlet mass flow ratio and at two immersions for various inlet mass flow ratios. Tests were made to determine the internal pressure recovery statically and dynamically. For these tests, pressures were sensed both at the inlet system diffuser and by means of a rake, at the model exit. A bell mouth inlet has been tested statically to establish a tare pressure recovery for the facility diffuser. The inlet cross-section, length and lip shape have been varied to determine the optimum final model configuration.

A movable, transparent viewing plate is employed for observation of flow condition within the water stream. In some photographs, the intersection of the water surface with the viewing plate could be mistaken for a bow wave ahead of the model, see Figure 11 for example.

5. DISCUSSION OF TEST RESULTS

The test results are intended to accomplish three distinct functions as follows:

a) Establish confidence in the vertical free jet facility and its instrumentation.

b) Provide performance data on various components which may be combined into a water scoop system.

c) Demonstrate the over-all performance of a typical scoop system.

The first two of these functions involve several families of simple component models, with each family contributing toward both functions. The discussion which follows is broken down by model type and frequent reference is made to pertinent results from the literature to indicate the degree of correlation between the present results and those of other workers in the field.

INLET MODELS

The thin wall inlet with a sharp lip is particularly interesting because its theoretical drag is so clearly defined, see Reference 5 for example. Figure 6 presents the measured drag coefficient of the sharp edged inlet model as a function of inlet velocity ratio. Nearly all the data points lie within $\pm$ 5% of the theoretical curve. This particular test involves measurement of free stream conditions, internal flow through the model, and model drags of about the design level, thus the $\pm$ 5% accuracy of this series may be

taken as representative of the accuracy of the entire test program,

The effect of rounding the lip of the thin wall inlet is also shown in Figure 6. Note that the cavitation bubble disappeared at $V_i/V_o = 0.5$ for both lip shapes, even though the drag levels clearly indicate loss of lip suction as a result of flow separation at that point. Throughout the test program, instances were found where a separated region sometimes filled with stagnant water and a visual check through the viewing plate would suggest that the flow was unseparated. The cavitation bubble could always be restored by additional ventilation. Drag effects arising from filling of the separated areas will be touched on in later sections. In the case of the thin wall inlet there is no significant drag change when the cavitation bubble disappears.

The drag of the ellipsoidal inlet model is shown in Figure 7 for three different lip shapes. At inlet velocity ratios above about 0.4, this model experiences a drag which is very nearly the sum of the ideal momentum drag plus the external drag of the ellipsoidal body from which it was derived. The drag due to flow separation (loss of lip suction) begins below $V_i/V_o = 0.4$ for the cavitated case, whereas in the absence of cavitation, flow separation seems to be absent above $V_i/V_o = 0.25$.

The inset in Figure 7 plots drag at zero internal flow vs. lip roundness ratio and suggests that an optimum occurs near $r/R = .05$. Note however that in the presence of cavitation (which must be assumed for a high

speed vehicle in normally rough water) and in the probable operating range between $V_i / V_o = 0.5$ and 0.7, the effect of lip shape is so small as to be negligible.

Photographs of the inlet models with and without cavitation may be found in Figure 8.

DRAG BODIES

Drag coefficients for a series of flat circular discs are presented in Figure 9a as a function of the ratio of disc diameter to jet diameter. Disc drag for this series ranges from 3% to 11% of the total jet momentum, yet the drag coefficients lie in the reasonably narrow region between $C_D = 0.82$ and 0.90. The drag correlation study of Figure 10 indicates excellent agreement between the present disc drag values and previously available tests and theories. Model drags up to 11% of the jet momentum are thus shown to be essentially free of jet size effects. No other models in the present program experienced drags greater than 5% of the total jet momentum.

Drag coefficients for three blunt based bodies of revolution are presented in Figure 9b as a function of Reynolds Number, although the narrow RN range of the present tests would not be expected to produce significant trends. Considerable scatter is evident in Figure 9b, most of which may be attributed to balance sensitivity, which was taxed by the very low drag level of these models. Even so, the drag of the cone correlates

well with other tests, Figure 10. The paraboloidal and ellipsoidal bodies are shown to offer progressive drag reductions as would be expected from theory, since a smaller trailing edge angle leads to a smaller cavitation bubble and drag at zero cavitation number can be related directly to bubble size.

As a matter of interest, the wakes of the drag bodies occasionally filled with water - in which case, the weight of the stagnant water was partially supported by low pressure on the model base and the drag reading was increased.

Photographs of several drag body tests are presented in Figure 11.

SURFACE PIERCING STRUT MODELS

Results of the strut tests are summarized in Figure 12. The circular cylinder struts were tested primarily for correlation purposes, and the results are shown to agree very well with Hoerner's $C_{D_{\pi'}} = .50$.

The three contoured models lead to some interesting conclusions. The wedge and ogive have substantially identical drag and the ellipse has considerably more drag. All three sections show a rapid build-up in drag as the tip is immersed to about d/w = 1.0, then they show linear behaviors to the maximum depth tested of d/w = 6.5. The ogive drag agrees well with Hoerner's result at d/w = 6.7.

NASA results, Reference 2, for airfoil sections tested at depths greater than d/w = 4 suggest that spray drag becomes constant at about d/w = 8 (this is borne out by their photographs as well as by the drag values shown in Figure 12). The spray photos of Figure 13 show rather clearly that spray intensity is increasing throughout the present test range, and the slopes of drag vs depth of Figure 12 appear to blend into the NASA slopes in the region of overlap near d/w = 6.5. It then appears that tip drag becomes established during the initial d/w = 1.0, spray drag becomes established by d/w = 6.0, and basic section drag prevails for deeper immersions. The ellipse causes greater spray drag by virtue of its blunt leading edge; however, it should offer lower section drag when fully immersed in accordance with incompressible fluid flow experience.

The strut immersion range of the present tests covers the region of interest for high speed scoops, and possibly some other applications as well. Any extrapolation of the present results to larger immersions should recognize the fact that the NASA results shown in Figure 12 are for complete airfoil sections, whereas the present models are blunt based.

PLANING MODELS

Lift and lift/drag data for the planing models are plotted in Figure 14 as functions of depth of immersion and trim angle. The lift results were quite repeatable and are believed to be accurate to $\pm$ 5%. The lift/drag ratios

are believed to indicate valid trends; however, the drag balance sensitivity was not adequate to define these values to an accuracy better than $\pm$ 10 to $\pm$ 15%.

The square planing surface results of Figure 14a may be compared with the partially immersed planing surface data of Reference 6 and with the fully immersed supercavitating hydrofoil data of Reference 7. Although not shown here, such a comparison has been performed and the agreement is satisfactory. No references are available for comparison in the transition region between partial and full immersion; however, the present results appear generally reasonable in this region.

Most of the models exhibited peculiarities in both lift and drag near the point of full immersion for trim angles near 6°. Not enough runs were made to define this situation completely, but there is a strong indication that various cavitation modes can exist in this vicinity. Shaded areas are shown in the data plots where the major ambiguities exist.

Summary comparisons of the various planing surfaces are presented in Figures 15a and b. Figure 15a is a composite of $\tau = 6^{\circ}$ results from the preceding plots.

In general, maximum L/D occurs near the point of full wetting of the lower surface. Only the flat disc shows a substantial improvement in L/D for larger immersions. Lift generally increases beyond the point of full wetting, with varying degrees of irregularity occuring near the fully-wetted point. The flat ellipse shows the smoothest lift build-up, while the cambered disc shows the greatest drop in lift after full wetting.

It should be noted that the cambered ellipse has simple curvature in the stream direction whereas the cambered disc is a spherical element and has variable camber along its span. This shape has been tested because of its great structural rigidity. It offers excellent performance near its design point but falls off severely during off-design operation.

Note that the L/D curves of Figure 15a represent the lower edge of the shaded regions of Figure 14. The higher values of L/D may well be obtainable in actual practice.

Figure 15b is based on a separate series of runs where the planing surface is maintained just at the point of full wetting while trim angle is varied. Results from Reference 7 are superimposed on the figure for comparison and the agreement for the square plate of AR = 1.0 is seen to be reasonable in view of the previously mentioned drag uncertainty. None of the present models match the L/D of the Tulin-Burkhart cambered surface, but the cambered disc and the high aspect-ratio ellipse approach it. The high aspect-ratio ellipse is uncambered and was obtained by a 90° rotation of the flat ellipse of Figure 14d. Photographs of various planing models may be found in Figure 16.

FINAL MODEL DESIGN

The complete inlet model shown in Figures 17 and 18 incorporates the following design features:

a) Rectangular internal flow passages to provide maximum flow area within minimum width.

b) Square inlet to simplify construction and to avoid a transition section.

c) Lip radius ratio, r/R = .05 from Figures 6 and 7.

d) Constant flow area from inlet through the bend to minimize frontal area.

e) No splitters within the bend. (Reference 4 shows this to be optimum for this duct.)

f) Gradual diffusion following bend.

g) Ogive strut contour for minimum strut drag. (The strut has a thickness ratio of about 30%, which is more than the 15% of the struts of Figure 12 but which is very close to the optimum thickness ratio for minimum drag per unit of frontal area.)

h) Elliptical ski without camber. (The ski size and geometry have been chosen somewhat arbitrarily, since vehicle stability requirements would be involved in the selection of skis for an actual Hydrostreak vehicle.)

i) Ski trim angle of 6^{o} for maximum lift/drag ratio. (Figure 14)

j) Ski vertical location at the assumed nominal smooth water immersion depth of the inlet.

FINAL MODEL PERFORMANCE

The present test program is concerned with the drag, pressure recovery and lift of the inlet assembly. The test results are discussed in that order in the following paragraphs.

Final Model Inlet Drag

Drag coefficient based on inlet area is plotted vs inlet velocity ratio in Figure 19a for the configuration of Figure 17. The ski is not installed and depth of immersion is 2.00 inches (d/w = 1.89). Drag without lip cavitation is similar to the thin wall inlet test results of Figure 6, with loss of lip suction beginning to appear as V_i/V_o goes below about 0.5. However, drag with lip cavitation is higher than anything previously encountered. A variety of minor modification to the inlet lip contour and to the transition region between the inlet and the strut were completely ineffective in reducing the cavitated drag. Extension of the square inlet well forward of the strut leading edge resulted in an appreciable reduction in drag as shown in Figure 19b. Suprisingly, however, the solution of this drag problem was achieved with a circular inlet rather than the original square inlet, as shown by the lower curve of Figure 19b. There is no known result in the literature to suggest that a square cavitating shape has a higher drag coefficient than a circle. Moreover, a careful visual examination of the entire flow field failed to disclose any changes in flow patterns which could account for this marked drag effect. Circular inlet length was varied to establish the pattern

of drag coefficient vs inlet length (Figure 19b).

Unfortunately, the round inlet configuration was obstructed internally where it joined the basic model so that tests could not be made with internal flow. It is reasonable to assume, however, that this configuration with cavitation will continue to follow the no cavitation drag curve of the original configuration, as suggested in Figure 19a.

Careful comparison of all the inlet drag results of Figures 6, 7 and 19 suggests that there is considerable benefit from the continued external contouring of the elliptical body inlet model over and above the effects of lip leading edge radius. This philosophy is incorporated into the full-scale inlet design of Figure 23. Other ramifications of this design change are treated later as part of the pressure recovery discussion.

Photographs of the final model with and without cavitation bubble are presented in Figure 18.

Final Model Strut Drag

Drag vs depth of immersion is shown in Figure 20 for the initial configuration at V_i/V_o = 0.6 and 1.0. Inlet momentum drag has been subtracted and results are presented for both the cavitating and non-cavitating operation. The non-cavitating case, which is assumed to be indicative of cavitating operation with the extended circular inlet, is of primary interest. Note that at V_i/V_o = 1.0 the total configuration drag coincides almost exactly with

strut-alone drag from Figure 12. At this operating point, no lip suction is required to counteract pressure drag within the scoop and there is no evidence of interference between the inlet and the strut. At $V_i/V_o = 0.6$ the inlet drag is parallel to but higher than the referenced strut-alone drag. The drag increment can be attributed to lip suction loss due to flow separation and amounts to $\Delta C_{D_{w2}} = 0.10$. Referred to inlet area, this drag becomes $\Delta C_{D_{Ai}} = 0.16$, which is not excessive, but which can undoubtedly be further reduced by the changes in lip shape mentioned in the preceding paragraph.

Final Model Pressure Recovery

Model inlet pressure recovery is evaluated by two methods. The first consists of a total pressure traverse at the model mounting flange, with typical results shown in Figure 21a. The pressure profiles reflect an unfavorable interaction between the bend and the diffuser of the model as tested. The second pressure measurement is taken by a piezometer ring at the outlet of the discharge diffuser, Figure 3. A tare calibration of the pressure drop within the model support beam, load cell and discharge diffuser has been made by mounting a bell mouth inlet on the model mounting flange and drawing water through the system with the auxiliary pump. The upper pressure recovery curve of Figure 21b is corrected for the tare pressure drop. The difference in pressure drop between the rake and the discharge

diffuser outlet measurements must then reflect additional losses within the model support beam and discharge diffuser as a result of the adverse flow profile delivered by the model. The lowest curve of Figure 21b shows the pressure drop to be expected from the model bend and model diffuser separately, calculated by the methods of Reference 4. The adverse interaction effect is again emphasized. As mentioned earlier, the model does not incorporate diffusion prior to the bend in order to minimize the frontal area of the inlet portion. Furthermore, the lower unit is held short to minimize wetted area both inside and outside. The drag results point out the desirability of extending the inlet forward and of providing additional curvature behind the lip. The additional frontal area is within the cavitation bubble and is not objectionable. Accordingly, the full-scale design, Figure 23, has a substantial degree of diffusion prior to the bend. This lowers local dynamic pressure at the bend and directly reduces pressure loss due to the bend.

Any bend tends to concentrate low momentum fluid along its inner wall, as shown clearly in Figure 21a, and the resulting flow is difficult to handle in a diffuser. Placing the diffuser ahead of the bend will eliminate this problem. A constant section is provided in the full scale design beyond the bend, so that symmetrical flow should be delivered at the mounting flange.

Pressure recovery testing of the final inlet model without external flow shows that $\Delta H/q_i$, for $V_o = 0$, is about 0.04 higher than for $V_i/V_o = 0.6$. This additional pressure drop is chargeable to separation at the inlet lip and is considered reasonable. Thus, the lip radius of r/R of .05 appears to represent a good compromise for static and high speed vehicle performance.

Final Model Ski Effectiveness

Lift and lift/drag ratio based on incremental effects due to ski addition to the inlet model are plotted in Figure 22. Ski lift in the presence of the strut is somewhat less than for the isolated skis of Figure 14; however, the general trends are quite similar. Lift/drag ratio is also somewhat less than for isolated skis, but again the results are considered reasonable. The incremental L/D of 5.0 (with cavitation) is attractive for Hydrostreak stabilization skis and may provide an incentive to carry a significant portion of the vehicle weight on skis rather than on the pressurized air bubble.

The inlet model demonstrated a substantial amount of lift without the ski attached; however, time was not available to ascertain that this lift was not influenced by flow conditions beyond the model proper. Therefore basic model lift is not presented. The possibility of encountering appreciable lift should be considered in any inlet applications of this type.

FULL-SCALE INLET DESIGN

The full-scale inlet of Figure 23 follows the design philosophy

previously outlined for the final test model with certain changes which have been mentioned in previous discussion and are summarized here for convenience:

a) The inlet is circular and is carried well forward of the strut leading edge to avoid interference drag.

b) The inlet is contoured externally for a finite distance behind the lip to benefit from the lip suction advantages exhibited by the ellipsoidal inlet model.

c) Diffusion is provided in the lower portion of the inlet ahead of the bend to minimize bend loss and to avoid interaction between the bend and the diffusion.

d) A splitter is incorporated in the bend because the bend is now rectangular in cross-section.

e) The strut is shortened to a length more indicative of a typical vehicle. (The final model strut was longer because of installation problems within the test facility.)

IMPLICATIONS OF THE PRESENT RESULTS IN TERMS OF HYDROSTREAK VEHICLE PERFORMANCE

Hydrostreak vehicle performance analyses performed by this contractor have incorporated water scoop performance assumptions generally consistent with the design study of Reference 5. A comparison of the present results with that design study will then indicate the agreement between these results and the general body of Hydrostreak performance calculations.

Reference 5 considers a scoop with an inlet area of 0.2 ft^2 operating at V_i/V_o = 0.59 at a forward speed of 70 knots. The referenced configuration differs in detail from the present concept, but it is made up of the same general components and can be compared with a similarly sized inlet of the present design as follows:

	V_o = 70 knots, V_i/V_o = 0.59, A_i = 0.2 ft^2	
ITEM	Reference 5	Present Test Results
Inlet Momentum Drag	3120 lbs	3120 lbs
Inlet Additive Drag	280 lbs	450 lbs
Strut Drag	650 lbs	540 lbs
Ski Drag*	270 lbs	220 lbs
Total Scoop System Drag	4320 lbs	4330 lbs
Pressure Loss $\Delta H/q_o$	0.09	0.084

*Ski sized for 1100 lbs lift

The inlet momentum drag so overshadows the other drag items that minor differences are rendered completely unimportant. Only inlet additive drag appears higher from the present tests, and the results from the ellipsoidal inlet model as applied to the full-scale design should minimize or eliminate this difference. The present strut drag is considerably less than the estimate of Reference 5, in spite of the fact that the present design has a wider strut in proportion to the inlet size and is also more deeply immersed as compared here.

Inlet pressure recovery as measured during the present tests is better than that assumed in Reference 5. In addition, there is reason to believe that the modifications incorporated in the full-scale design will yield substantial further improvements.

In conclusion, the present test results appear to justify fully the scoop performance assumptions incorporated into previous Hydrostreak performance estimates.

6. CONCLUSIONS

1. The vertical free jet offers a simple and reliable test facility for small scale testing of high speed hydrodynamic configurations.

2. Lip drag can be reduced to $\Delta C_{D_{Ai}} = 0.16$ or below for useable inlet configurations.

3. Ogive strut drag is no higher in the presence of a properly located inlet than for an isolated strut configuration. For the inlet model tested, and for a typical depth of immersion, strut drag is approximately equal to inlet lip drag.

4. An uncambered elliptical ski will yield incremental lift/drag values of 5.0 or better when installed on an inlet strut. Cambered ski sections show promise of substantial improvements above this level.

5. At an inlet Vi/Vo = 0.6, internal pressure losses in a well designed inlet will be no greater than 8.5% of free-stream dynamic pressure - again much improvement is possible.

6. The present test results justify the inlet performance assumptions made in previous Hydrostreak vehicle performance estimates.

7. REFERENCES

1. Hoerner, S. F., Fluid Dynamic Drag, 1958 Edition

2. Coffee, C. W., Jr. & McKann, R. E., NACA Technical Note 3092, Hydrodynamic Drag of 12 and 21 Percent Thick Surface Piercing Struts.

3. Streeter, V. L., Fluid Dynamic Handbook.

4. SAE Aero-Space Applied Thermodynamics Manual.

5. Devault, R. T., Design Study of Water Scoops for Hydrostreak Craft, Report HTC-60-3, Hughes Tool Company - Aircraft Division.

6. Weinstein, I. & Kapryan, W. J., NACA Technical Note 2981, The High-Speed Planing Characteristics of A Rectangular Flat Plate Over A Wide Range of Trim and Wetted Length.

7. Johnson, V. E., Jr., NASA Technical Report R-93, Theoretical and Experimental Investigation of Supercavitating Hydrofoils Operating Near The Free Water Surface.

8. Breslin, J. P. & Skalak, R., NASA Technical Report R-86, The Drag Coefficient of Parabolic Bodies of Revolution Operating At Zero Cavitation Number and Zero Angle of Yaw.

ACKNOWLEDGEMENT

Special mention must be made of the contributions of Mr. R. Heacock during the initial facility design and of Mr. J. W. Cornell during the entire facility construction and test program.

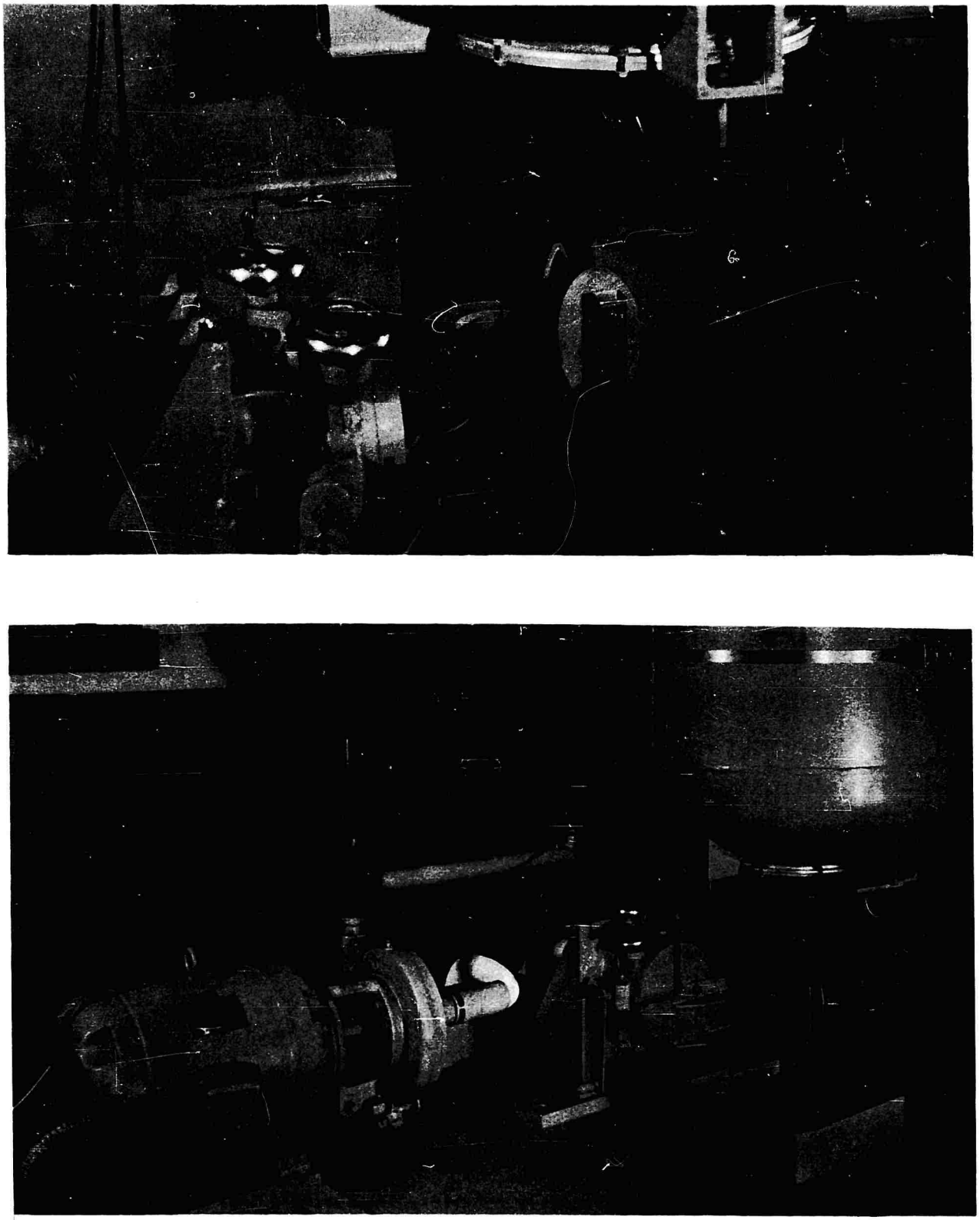

Figure 1. Hughes Hydrodynamics Laboratory

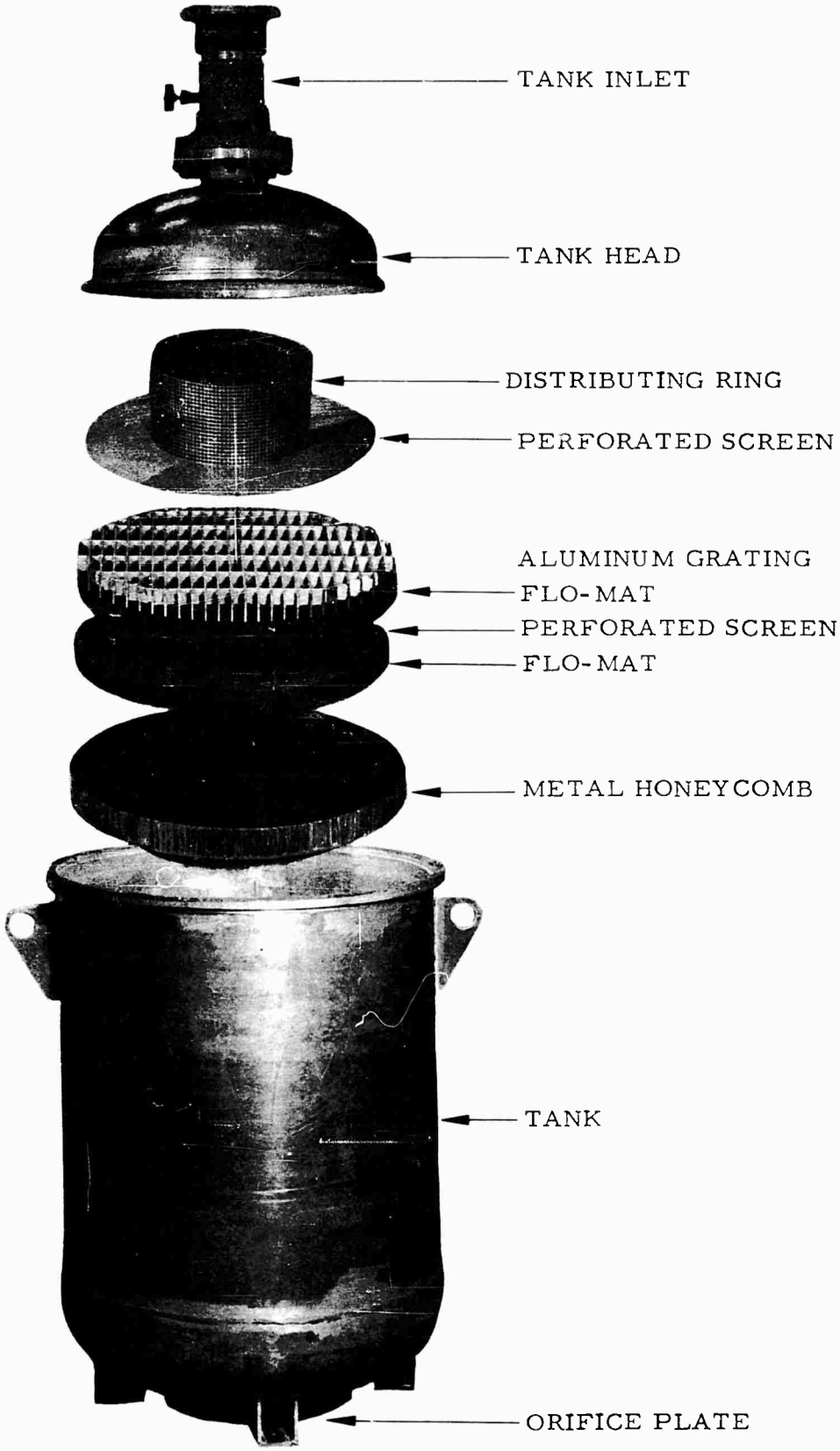

Figure 2. Stilling Chamber Assembly

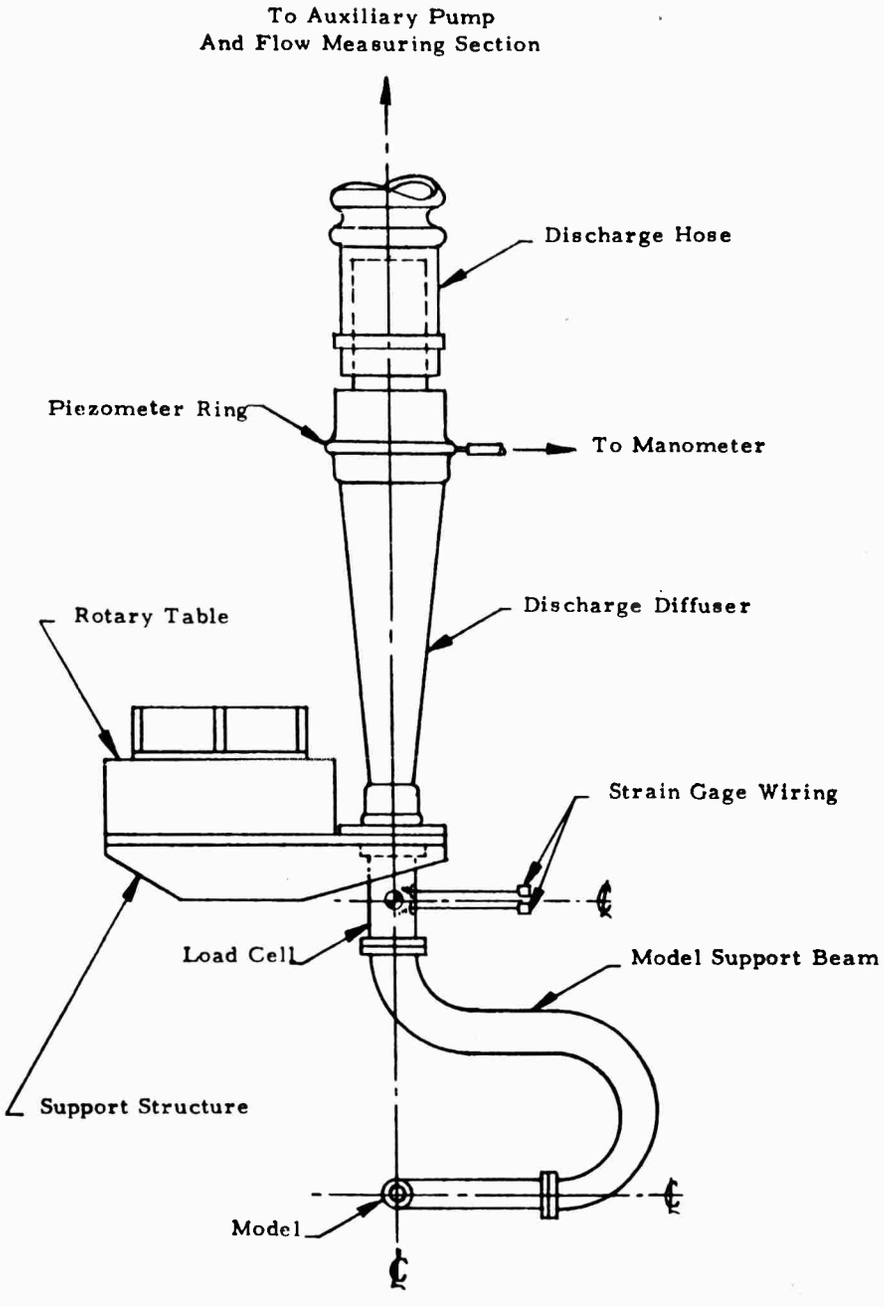

Figure 3. Internal Flow and Force Measuring System

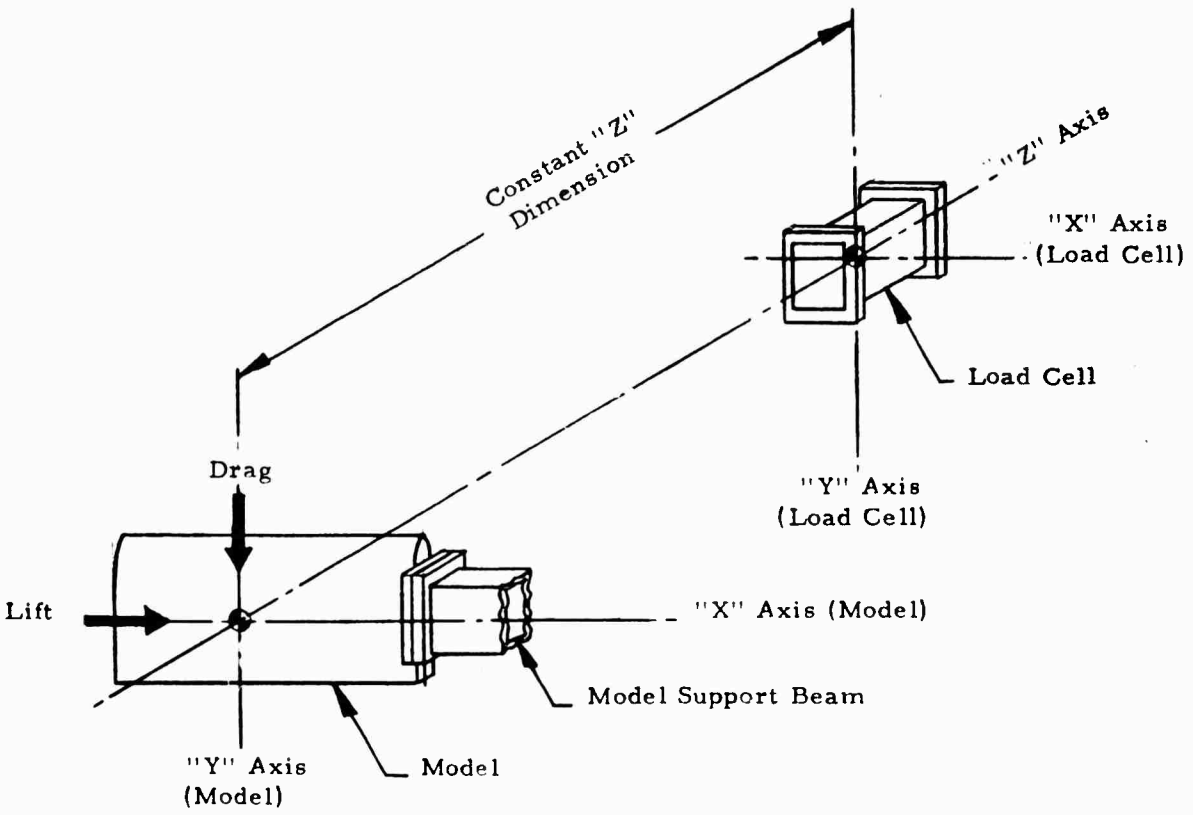

Figure 4. Force Measuring System

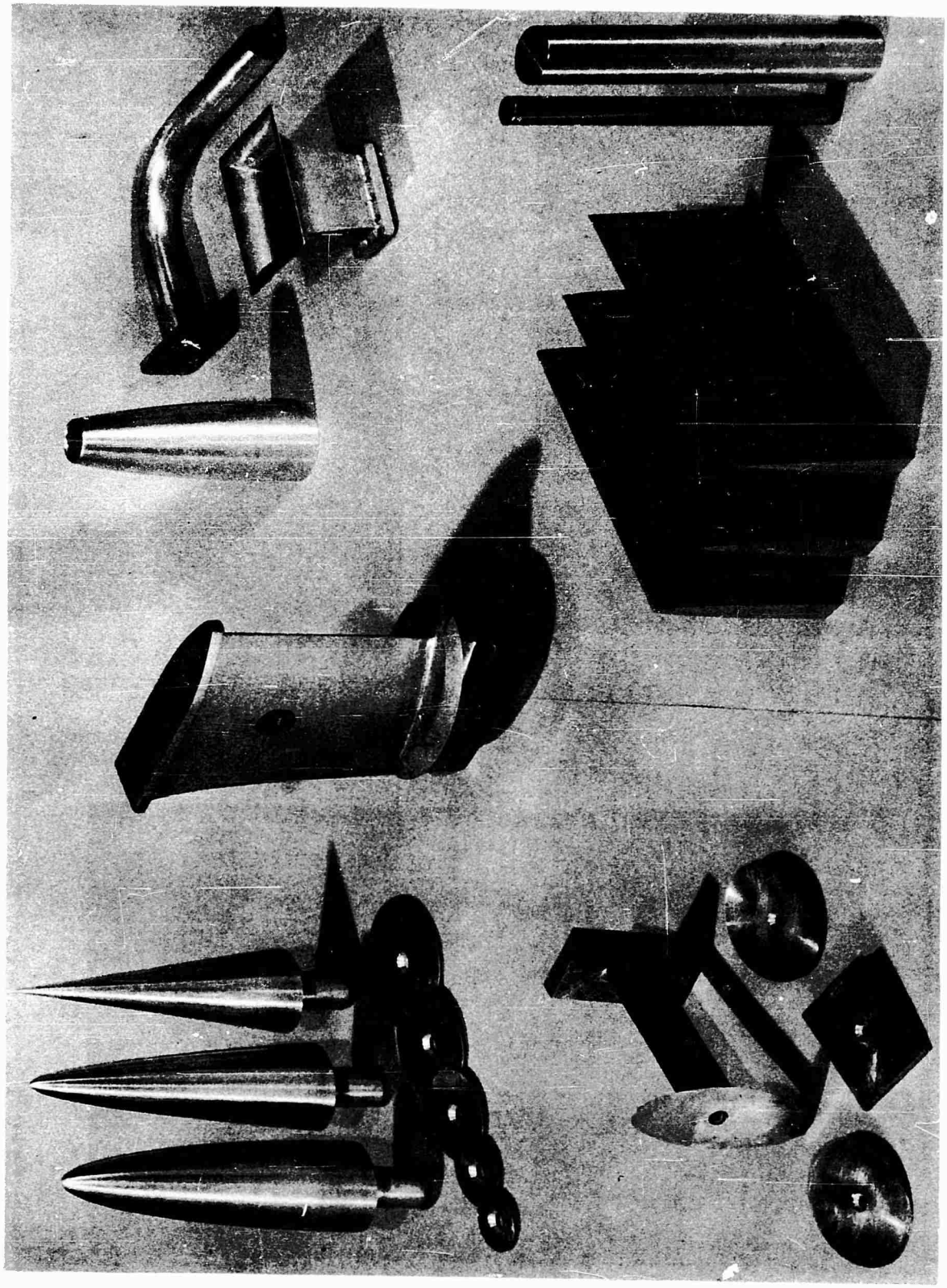

Figure 5. Models

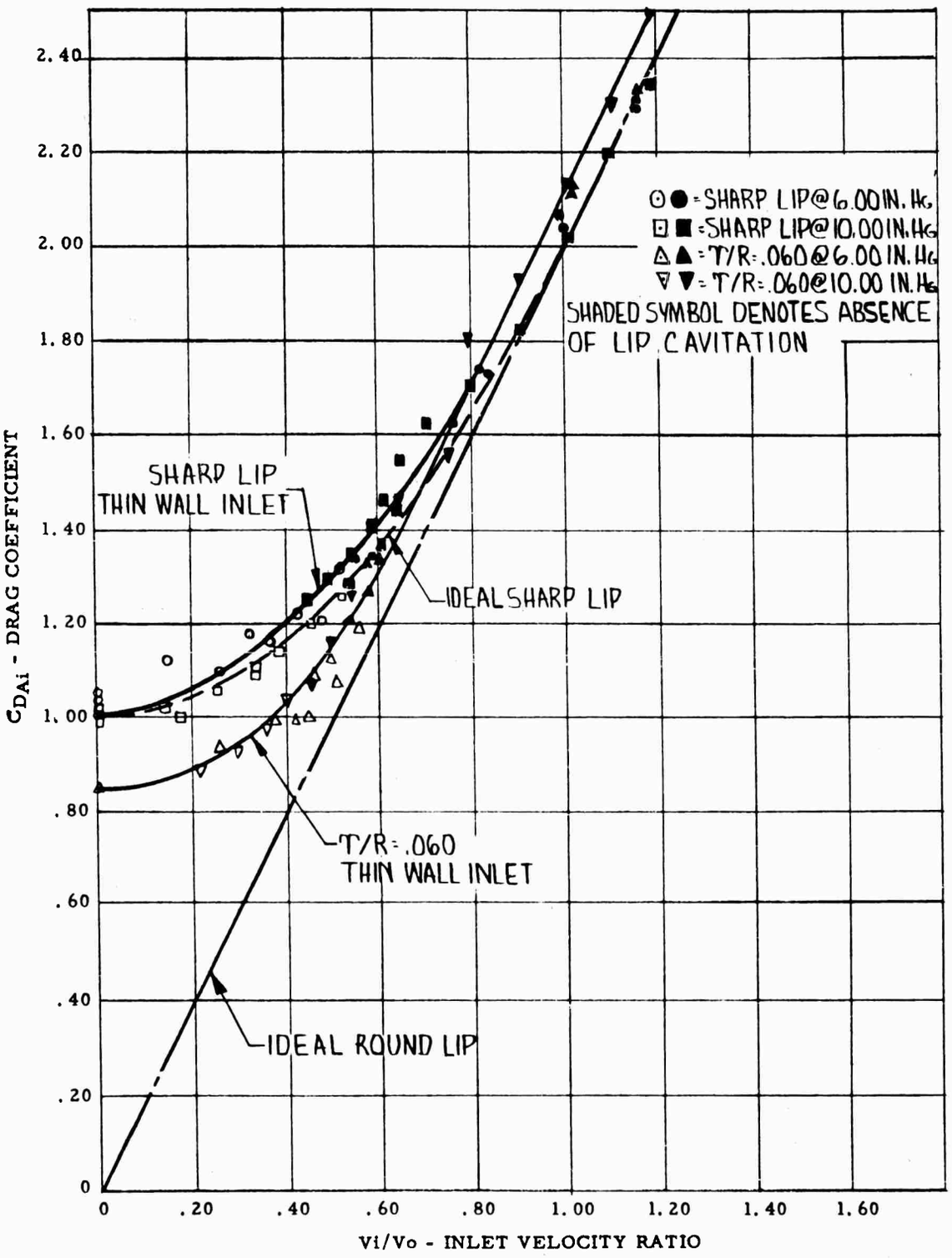

Figure 6. Thin Wall Inlet

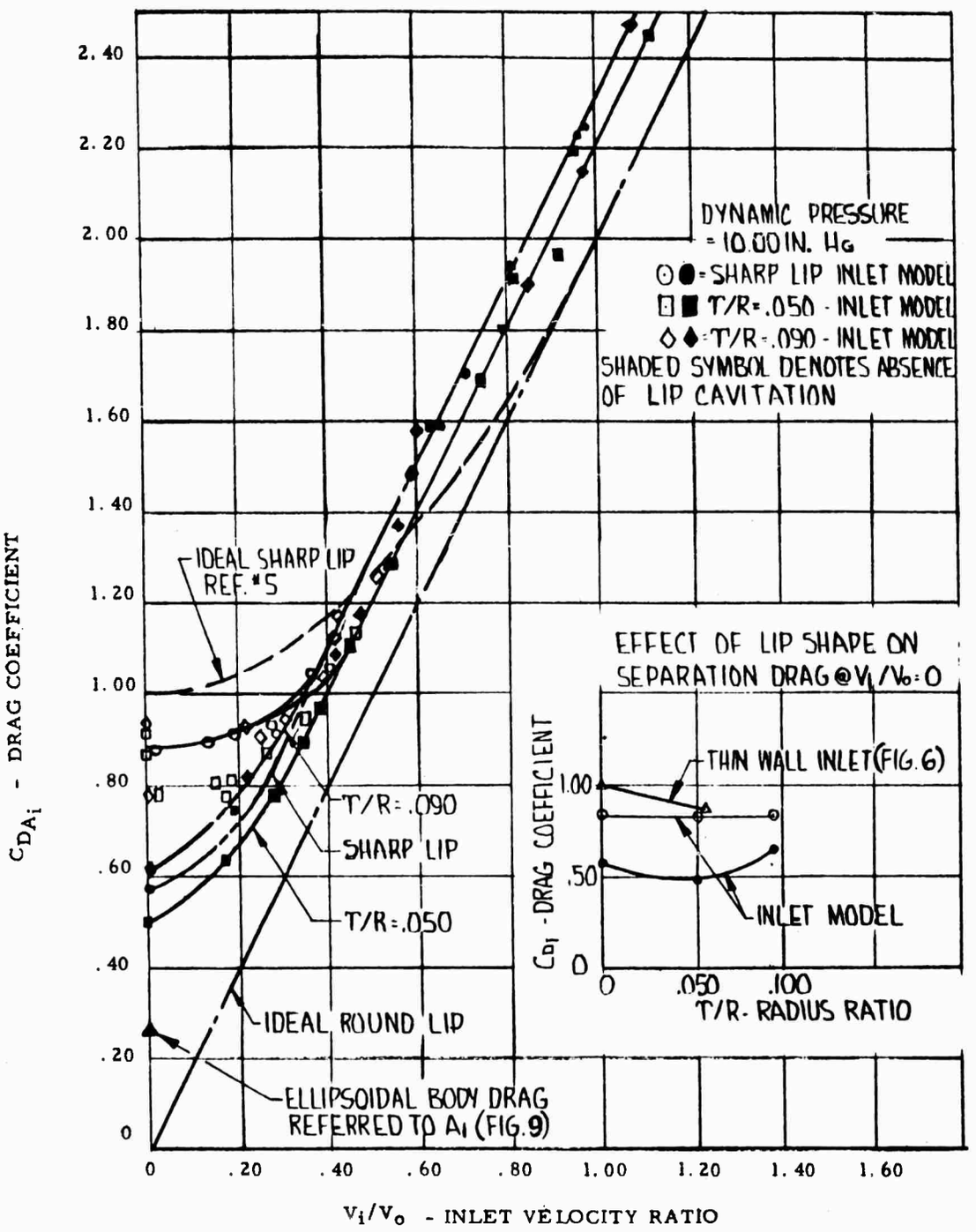

Figure 7. Ellipsoidal Inlet Model

a) THIN WALL INLET

b) THIN WALL INLET

c) DRAG DISC

d) INLET MODEL

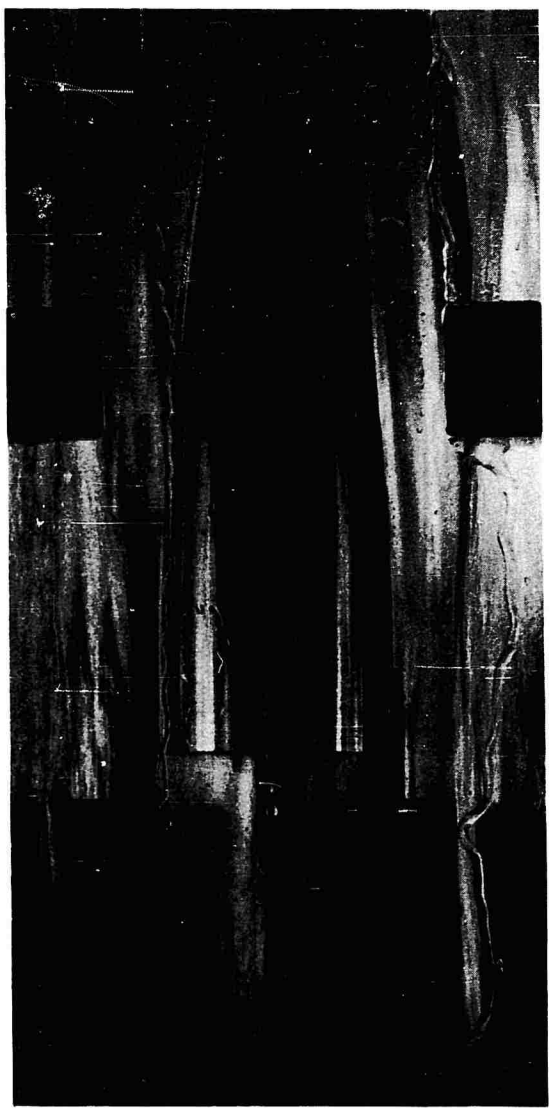

e) INLET MODEL

Figure 8. Thin Wall Inlet, Drag Disc & Inlet Model

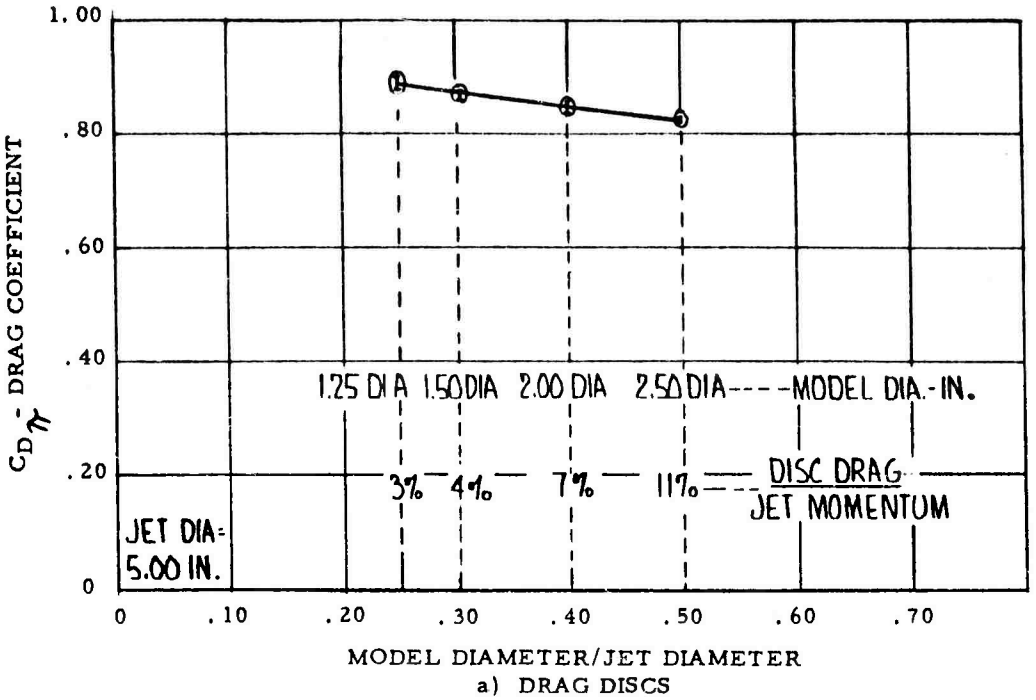

a) DRAG DISCS

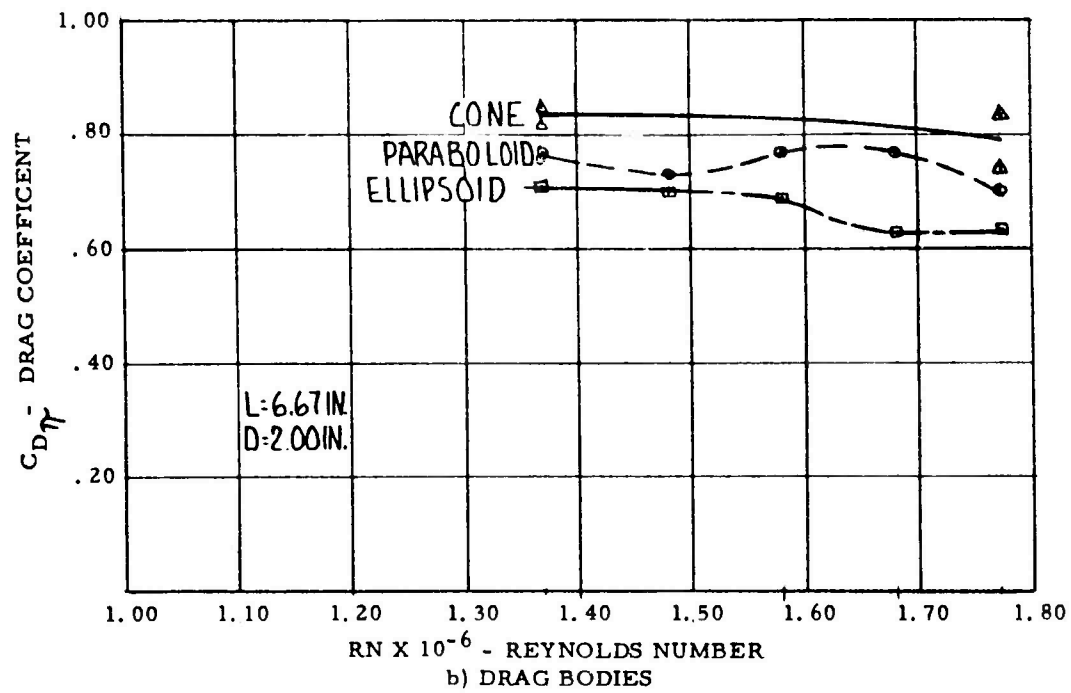

b) DRAG BODIES

Figure 9. Drag of Circular Discs and Bodies of Revolution

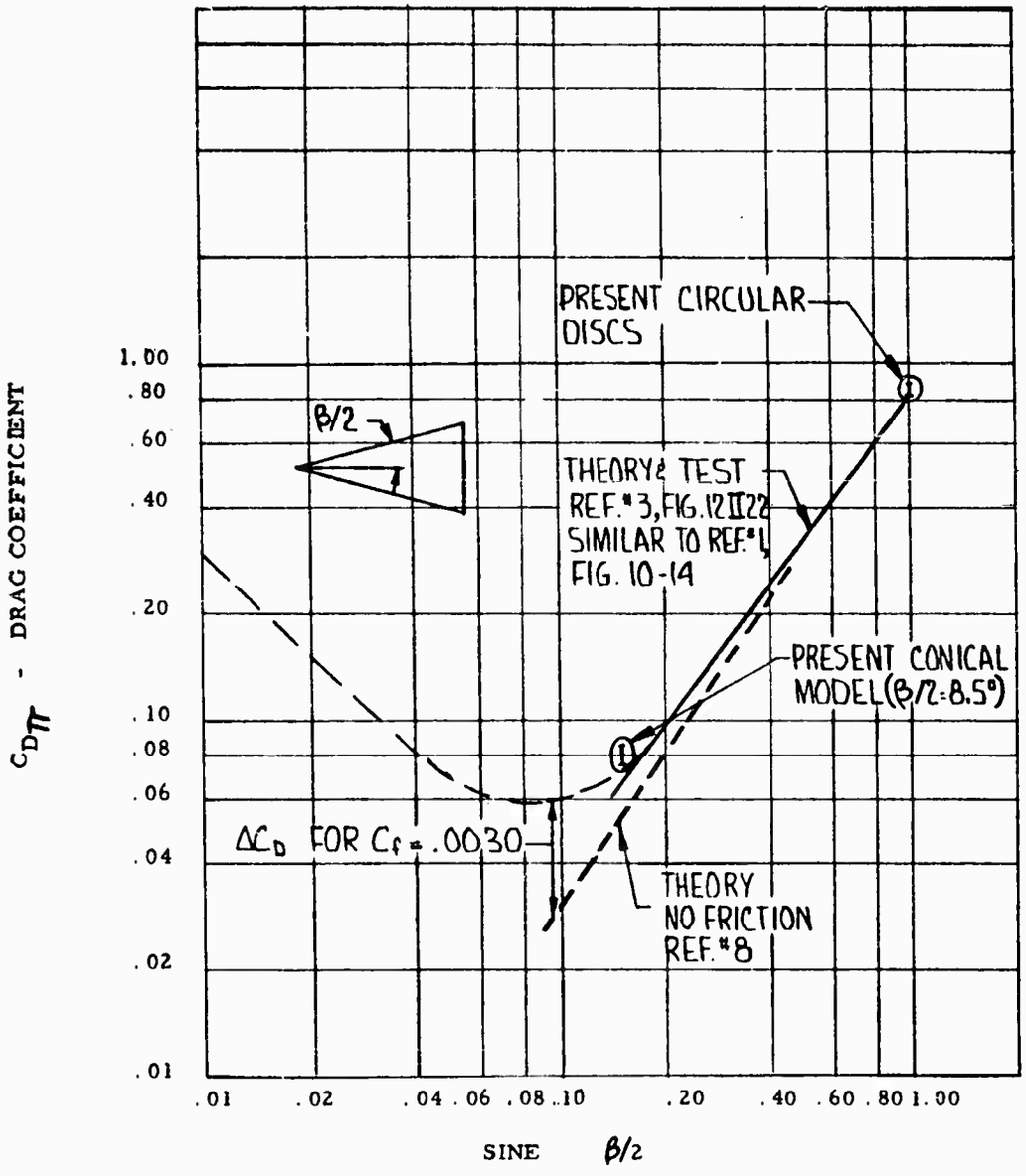

Figure 10. Drag of Conical Bodies

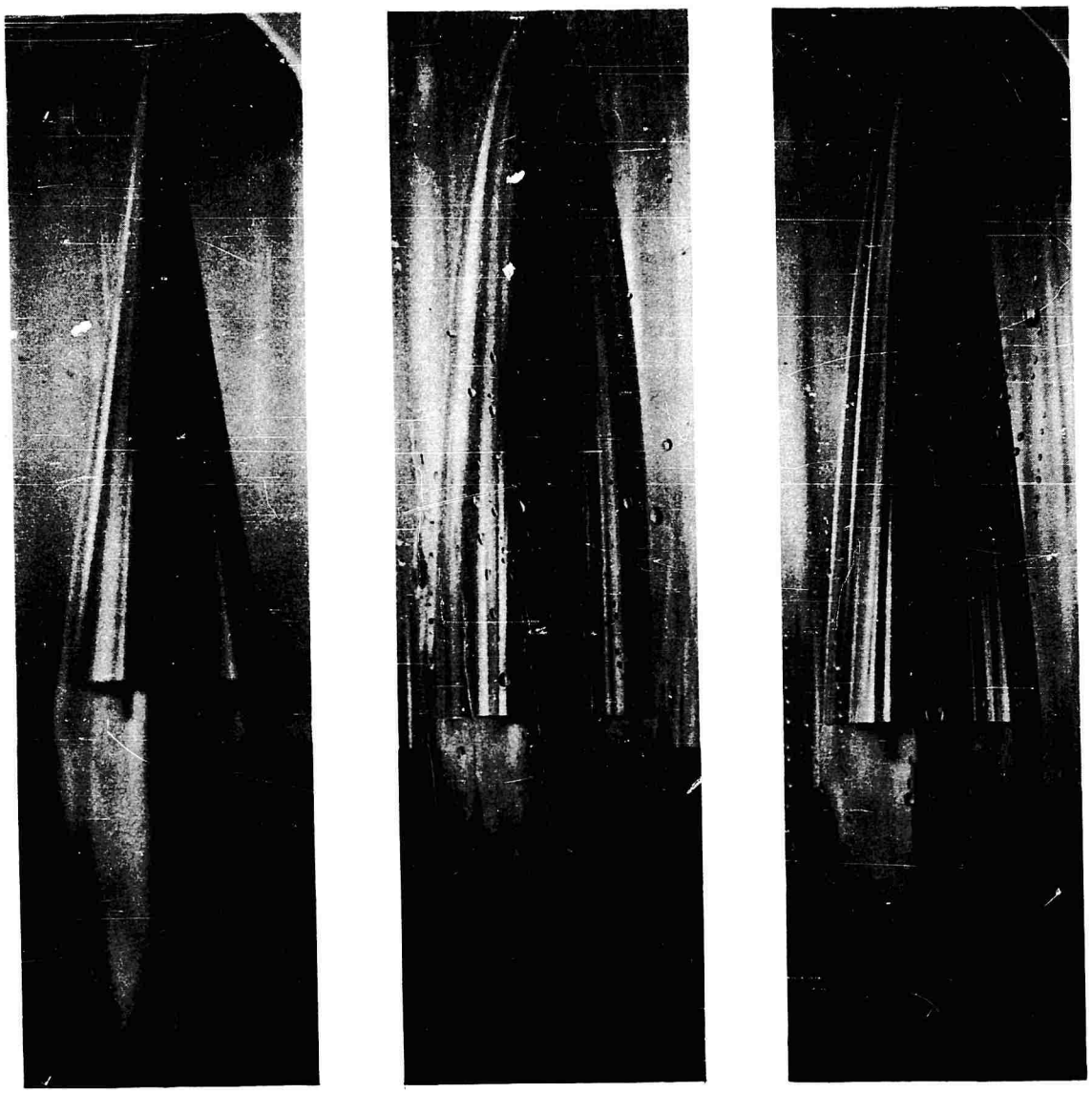

a) CONE b) ELLIPSOID c) PARABOLOID

Figure 11. Drag Bodies

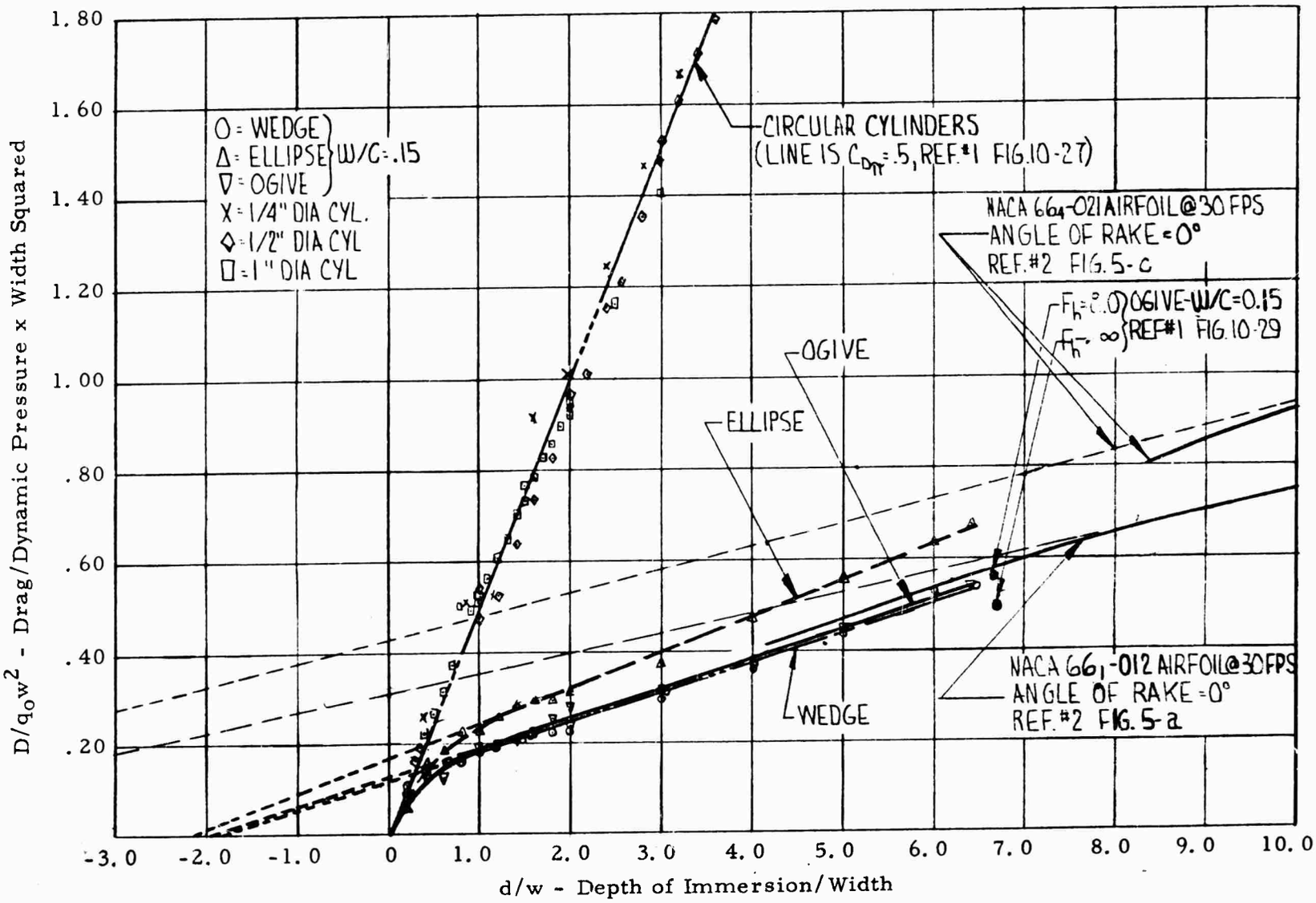

Figure 12. Strut Models

a) OGIVE

b) CIRCULAR CYLINDER

c) OGIVE - SHALLOW IMMERSION

d) CIRCULAR CYLINDER - SHALLOW IMMERSION

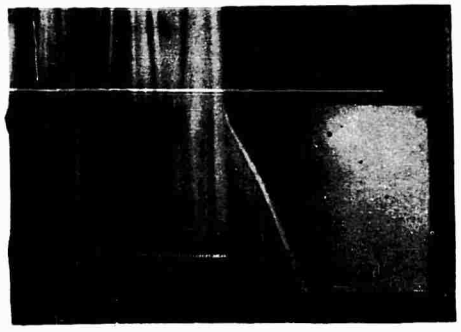

e) OGIVE - DEEP IMMERSION

f) CIRCULAR CYLINDER-DEEP IMMERSION

Figure 13. Strut Models

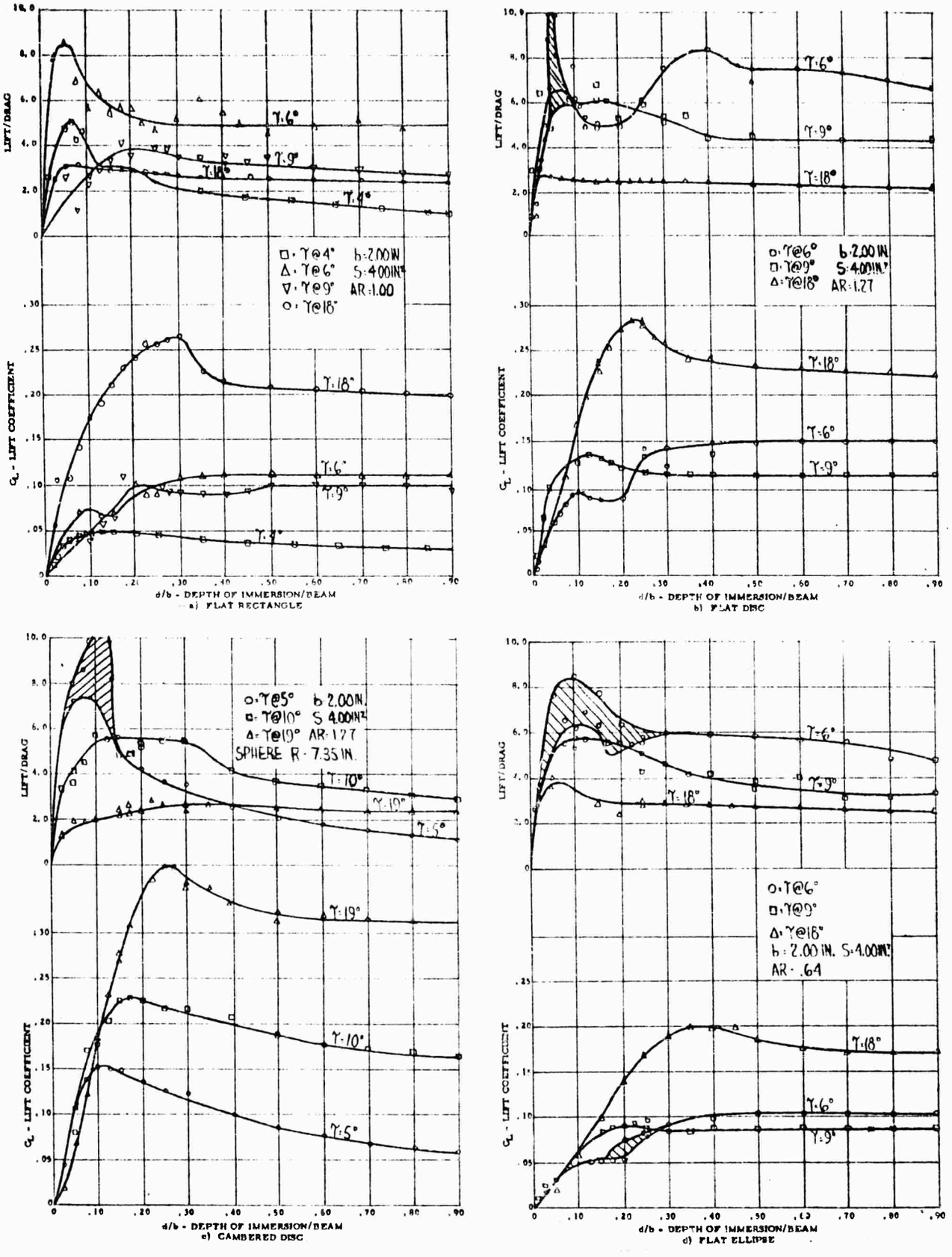

Figure 14. Lift and Drag of Planing Surfaces

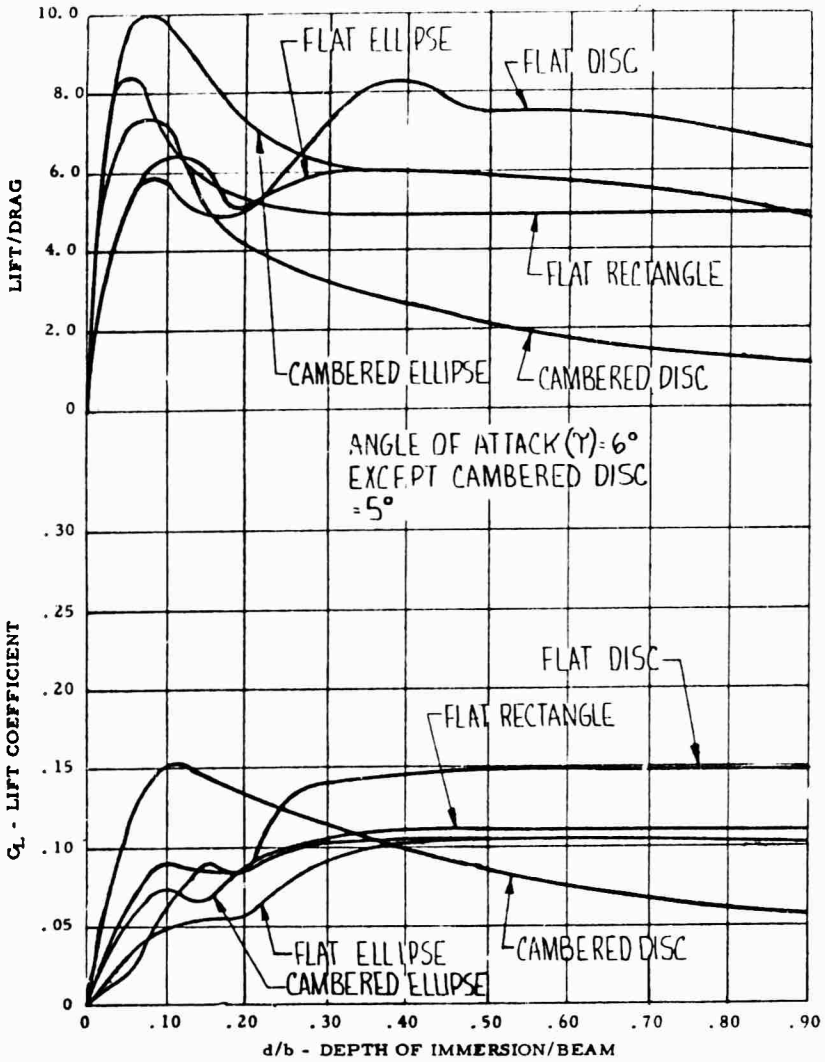

(a) COMPARISON OF PLANING MODELS AT OPTIMUM ANGLES OF ATTACK

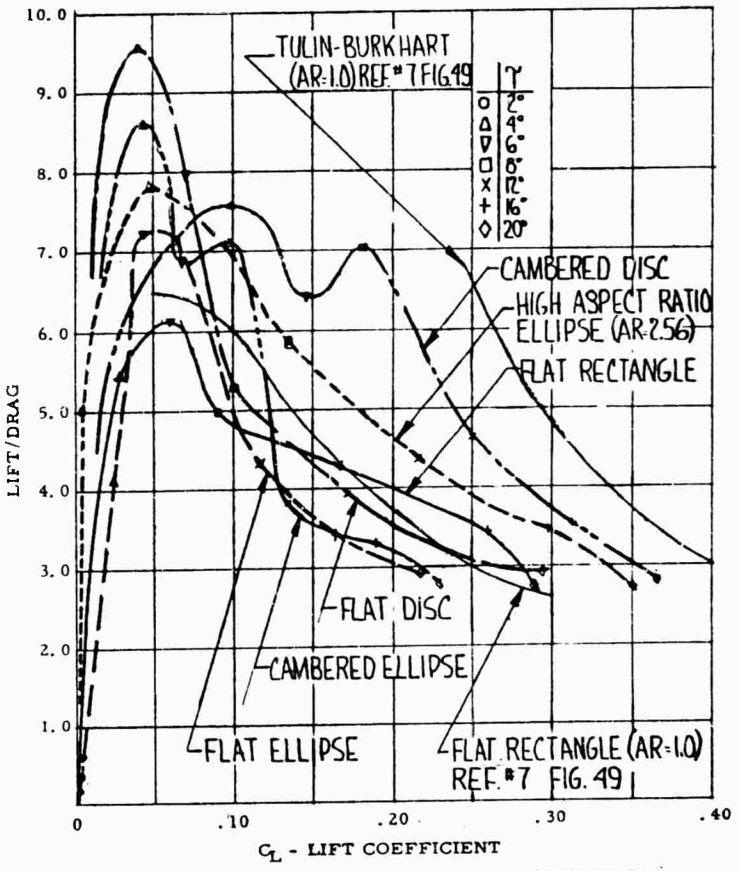

(b) COMPARISON OF FULLY WETTED PLANING MODELS

Figure 15. Comparison of Planing Models

a) RECTANGULAR PLATE

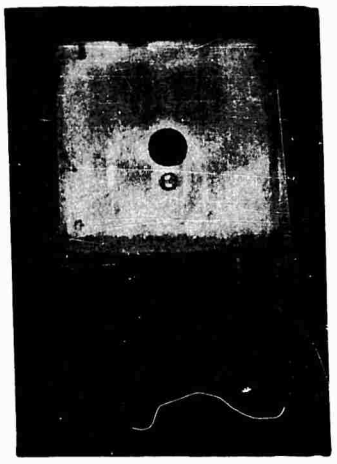

b) RECTANGULAR PLATE

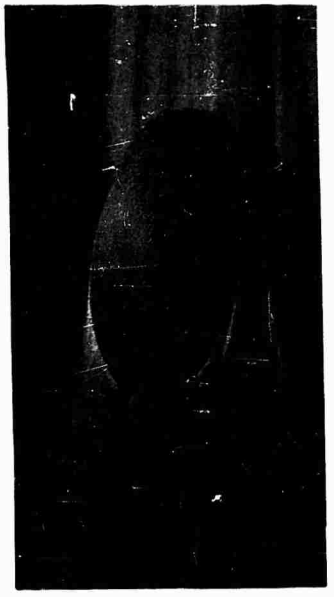

c) CAMBERED DISC

d) FLAT DISC

e) FLAT ELLIPSE

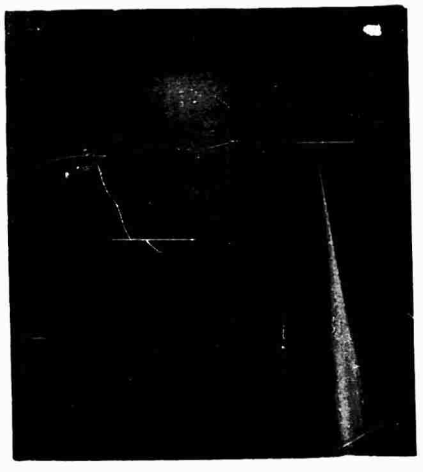

f) CAMBERED DISC

Figure 16. Planing Models

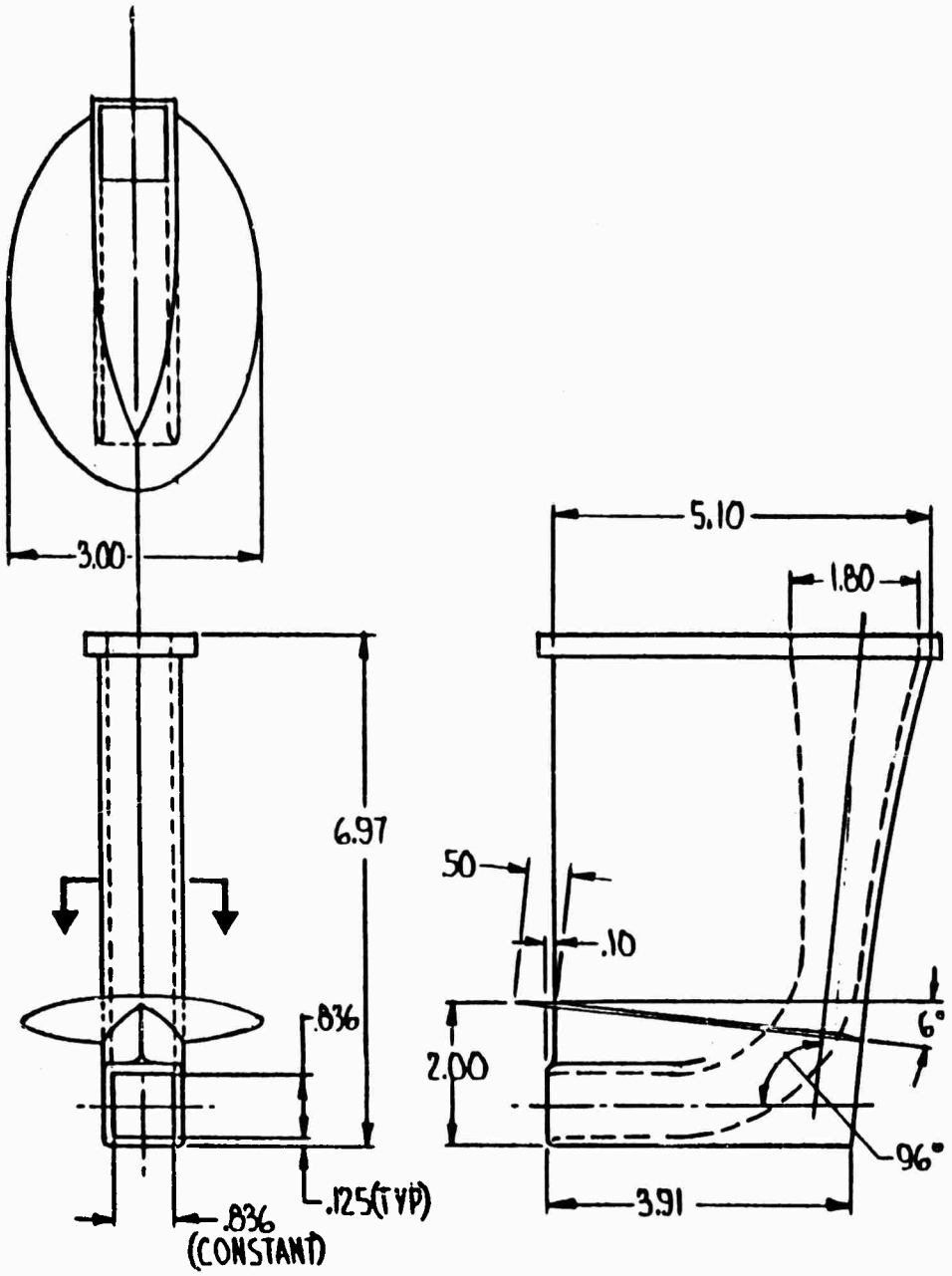

Figure 17. Final Model

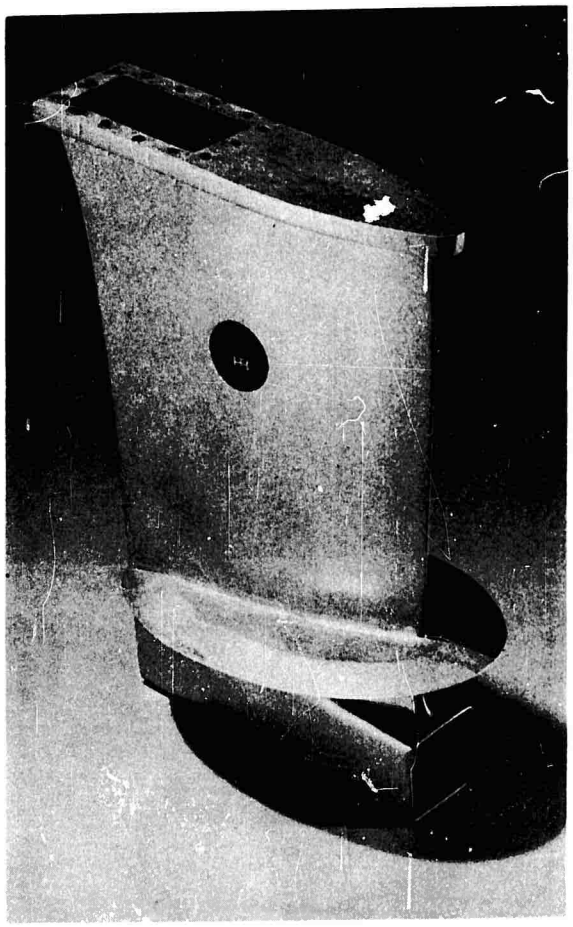

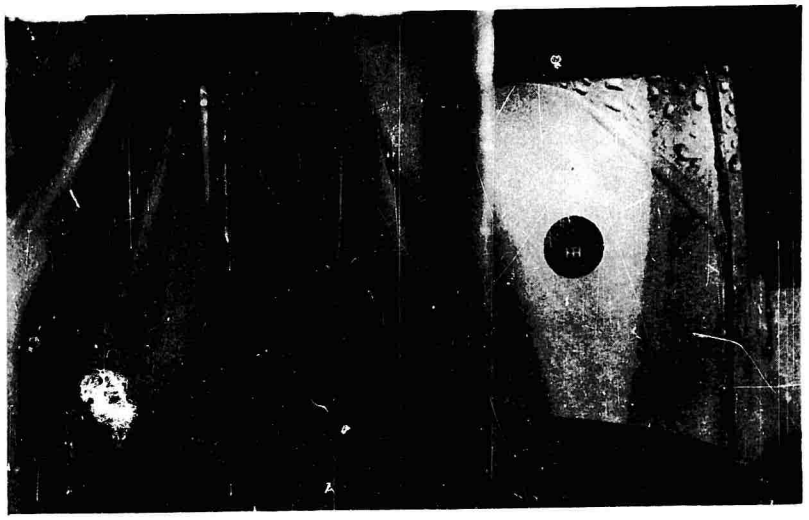

a) WITH LIP CAVITATION

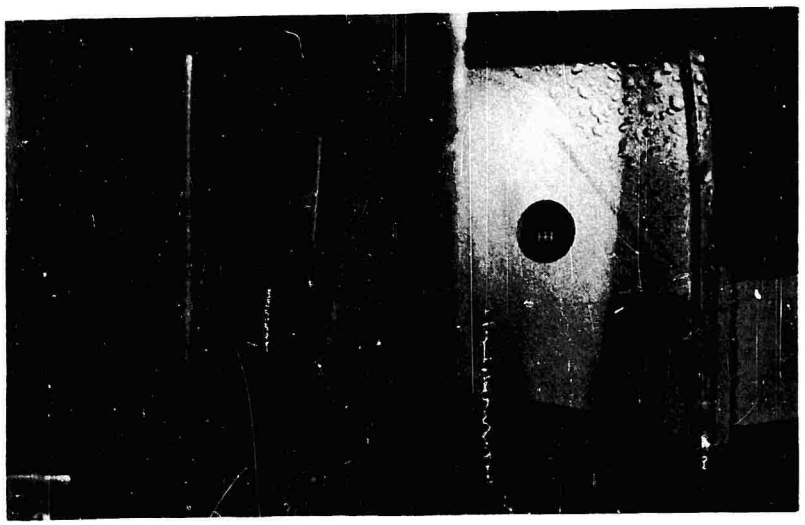

b) WITHOUT LIP CAVITATION

Figure 18. Final Model

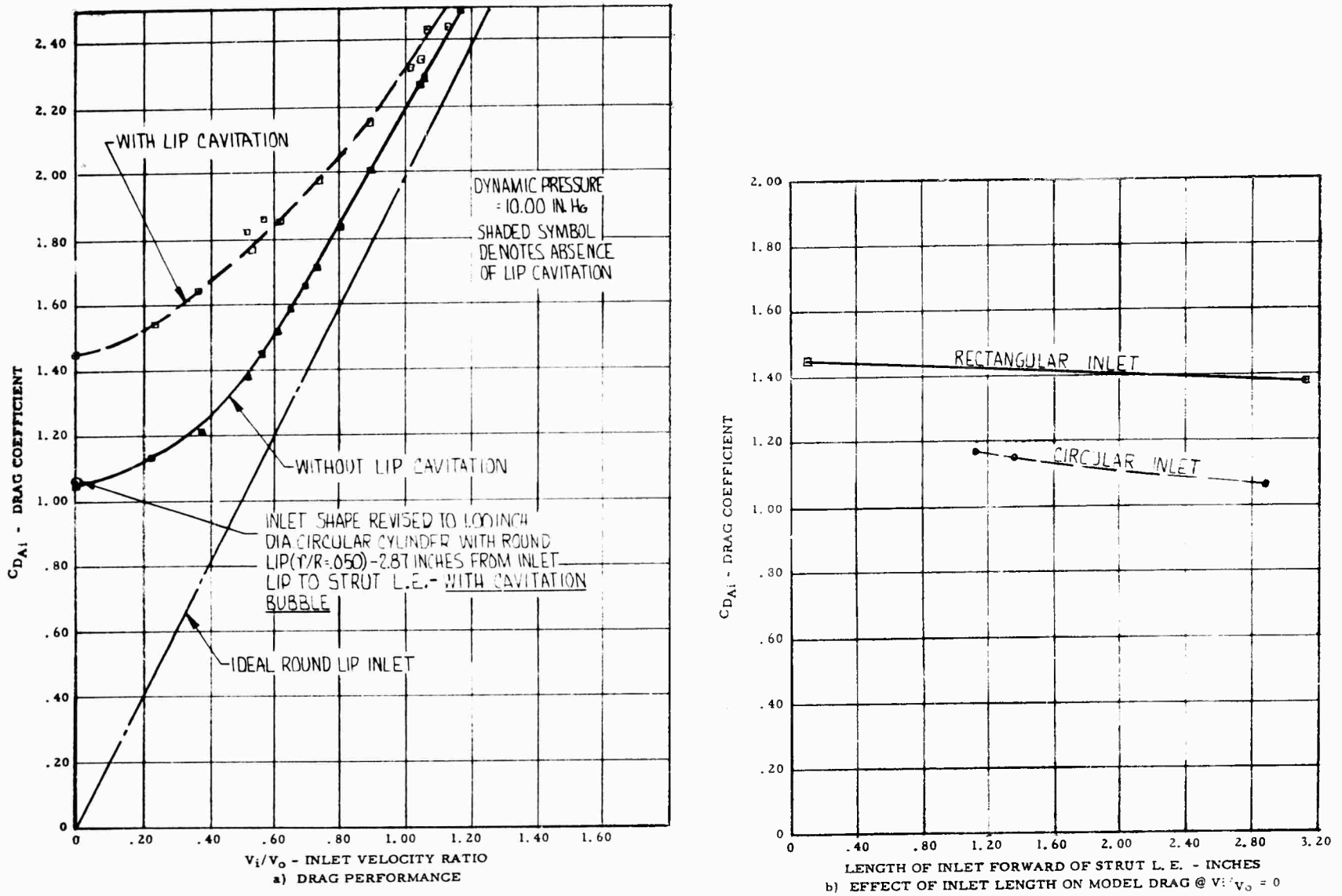

Figure 19. Final Model Inlet Drag

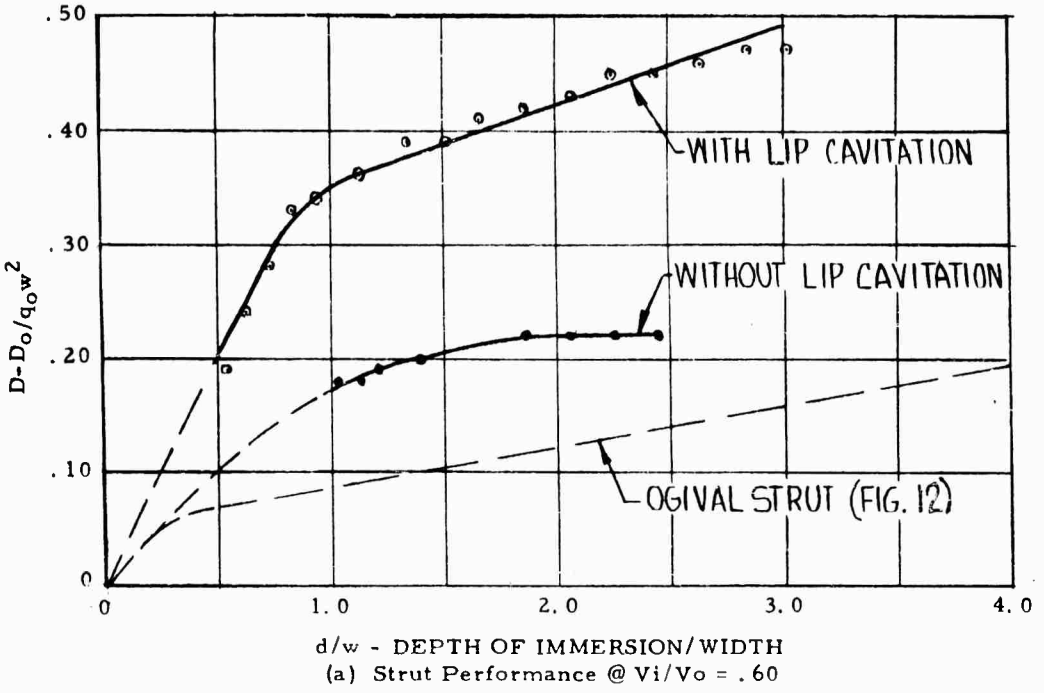

(a) Strut Performance @ Vi/Vo = .60

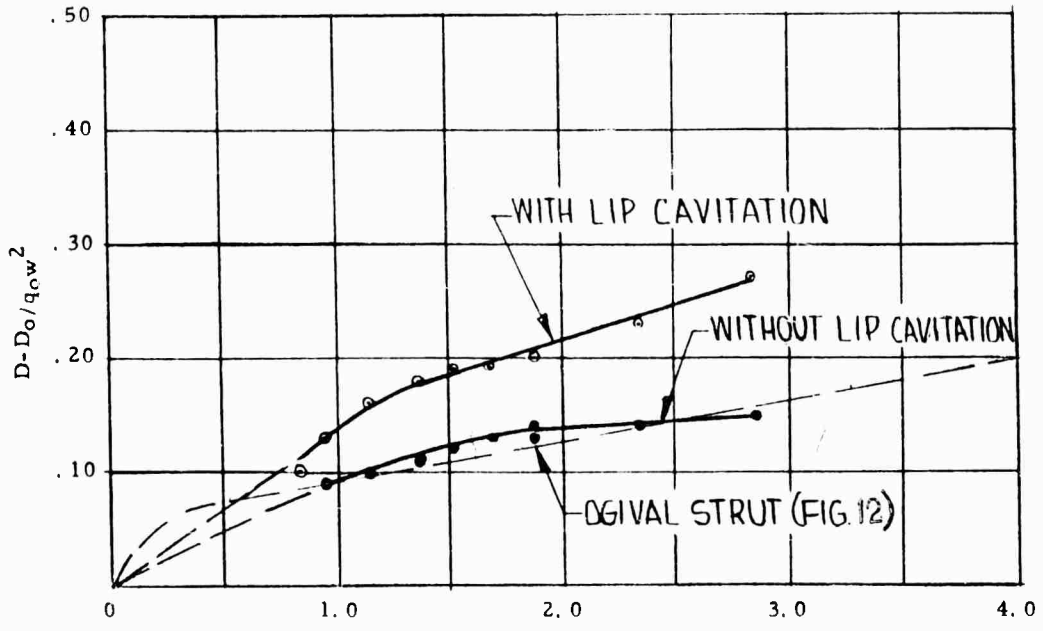

(b) Strut Performance @ Vi/Vo = 1.00

Figure 20. Final Model Strut Effectiveness

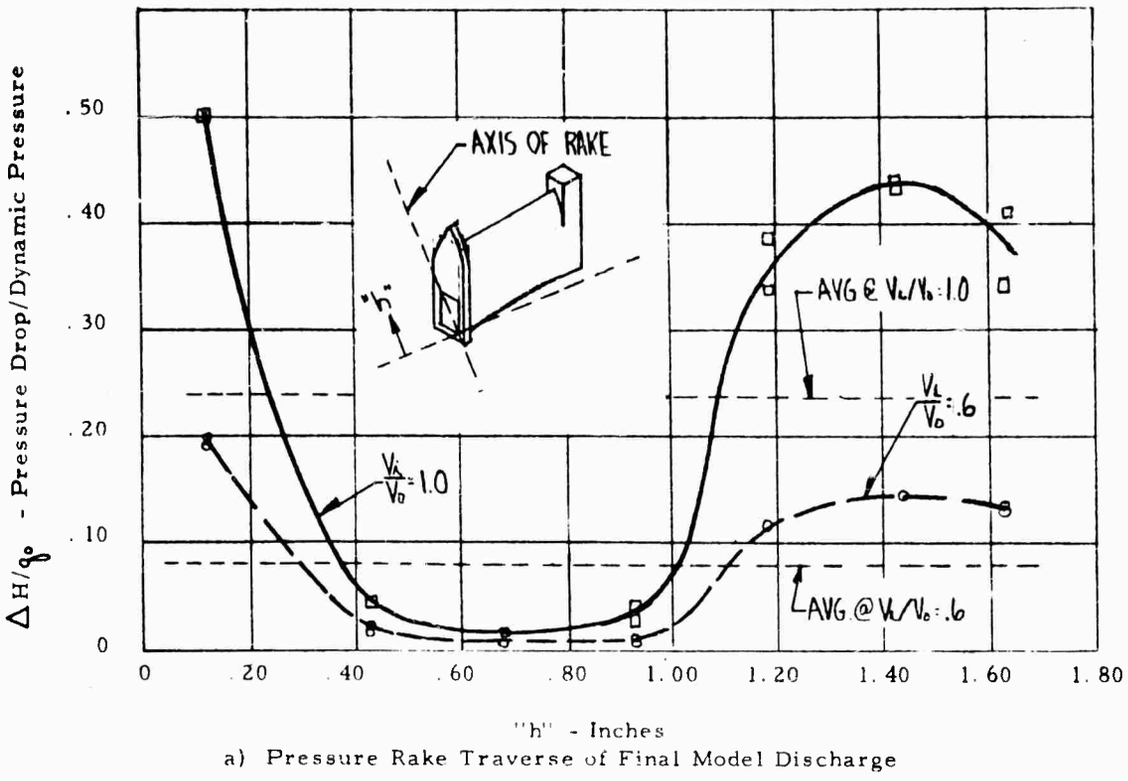

a) Pressure Rake Traverse of Final Model Discharge

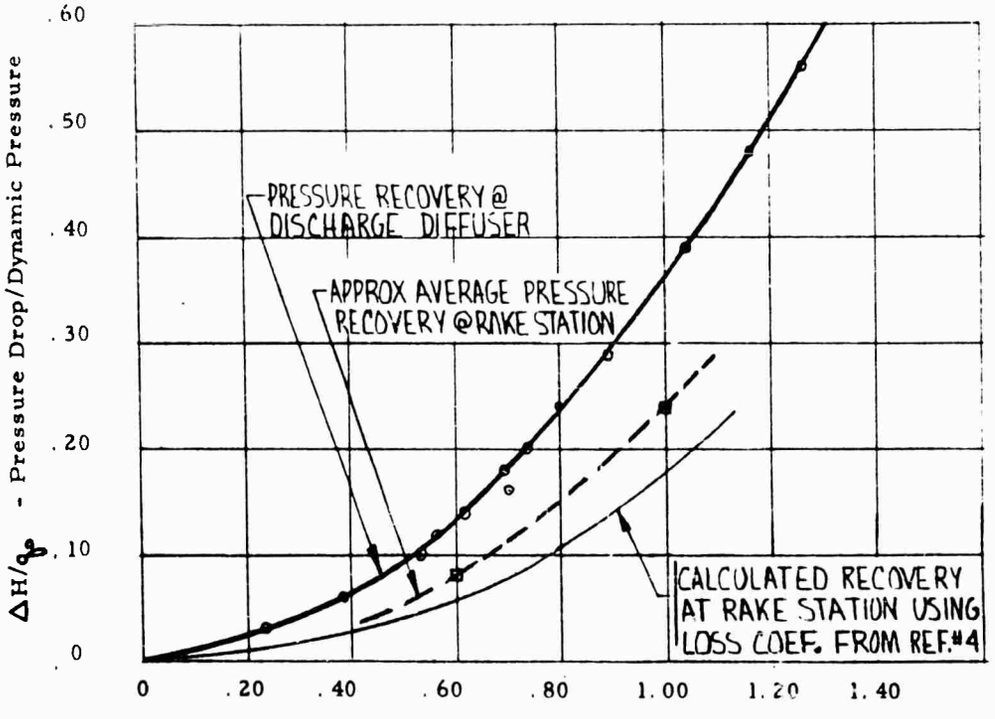

b) Inlet Pressure Recovery

Figure 21. Final Model Internal Performance

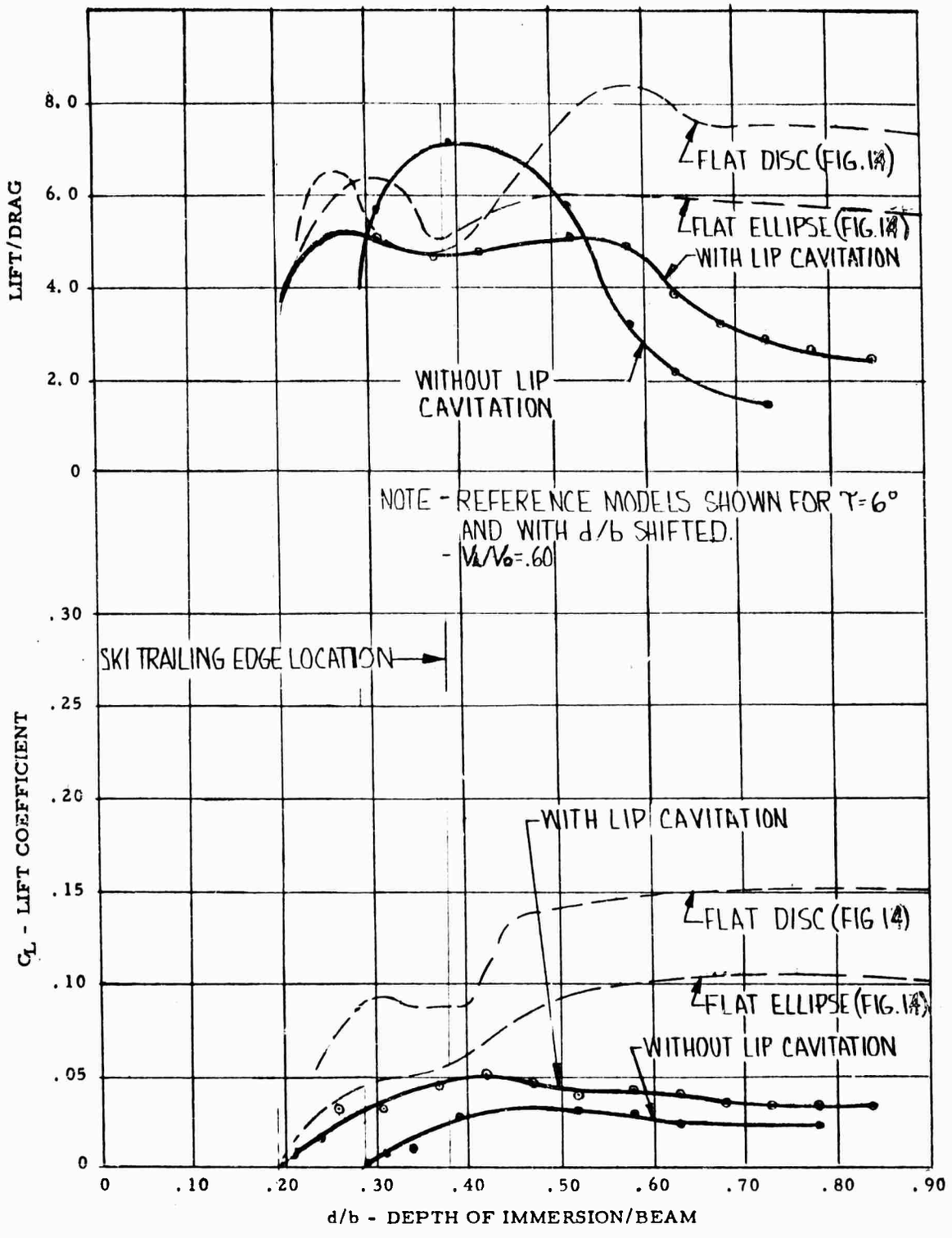

Figure 22. Final Model Ski Effectiveness

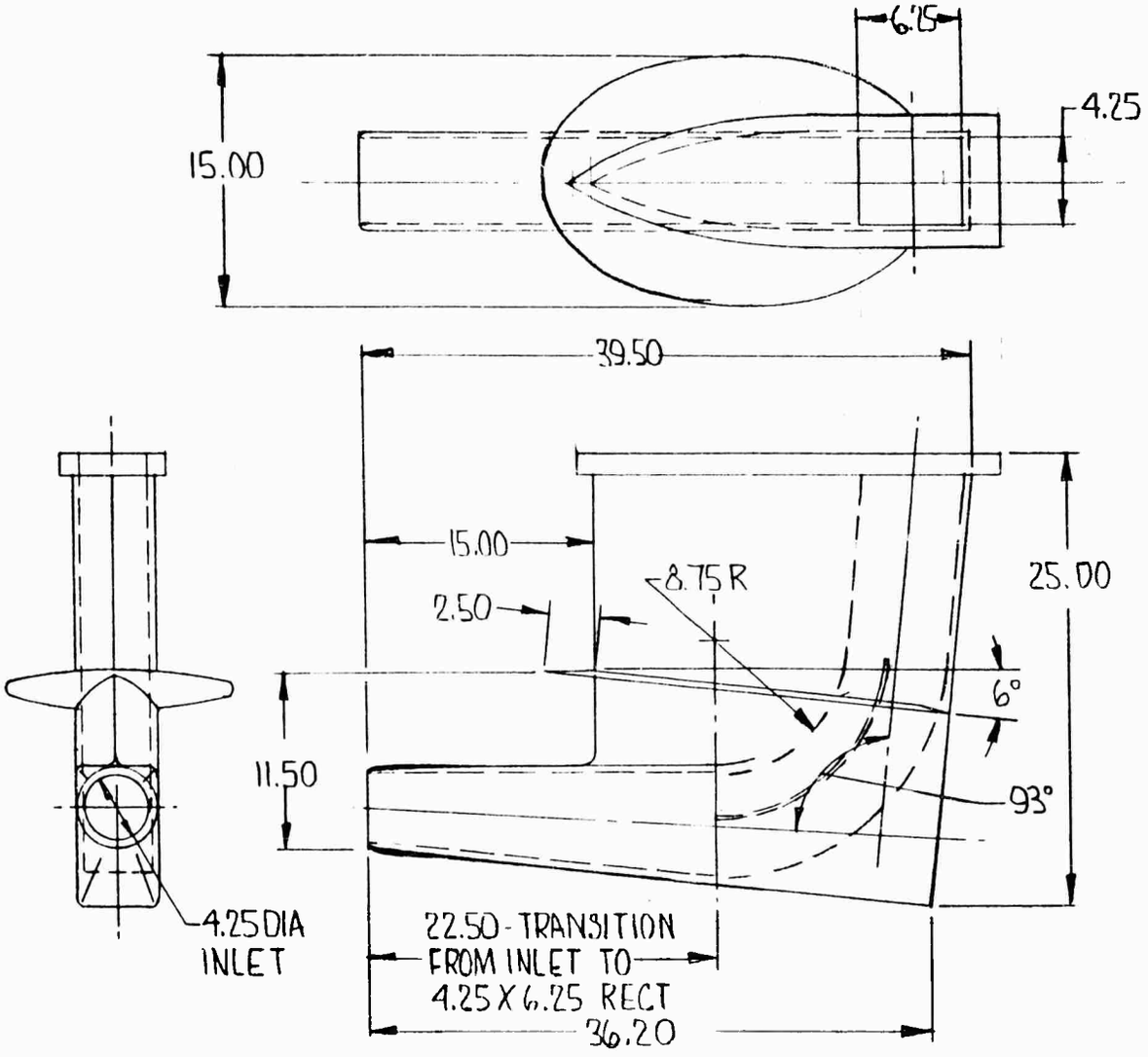

Figure 23. Recommended Full Scale Scoop Design

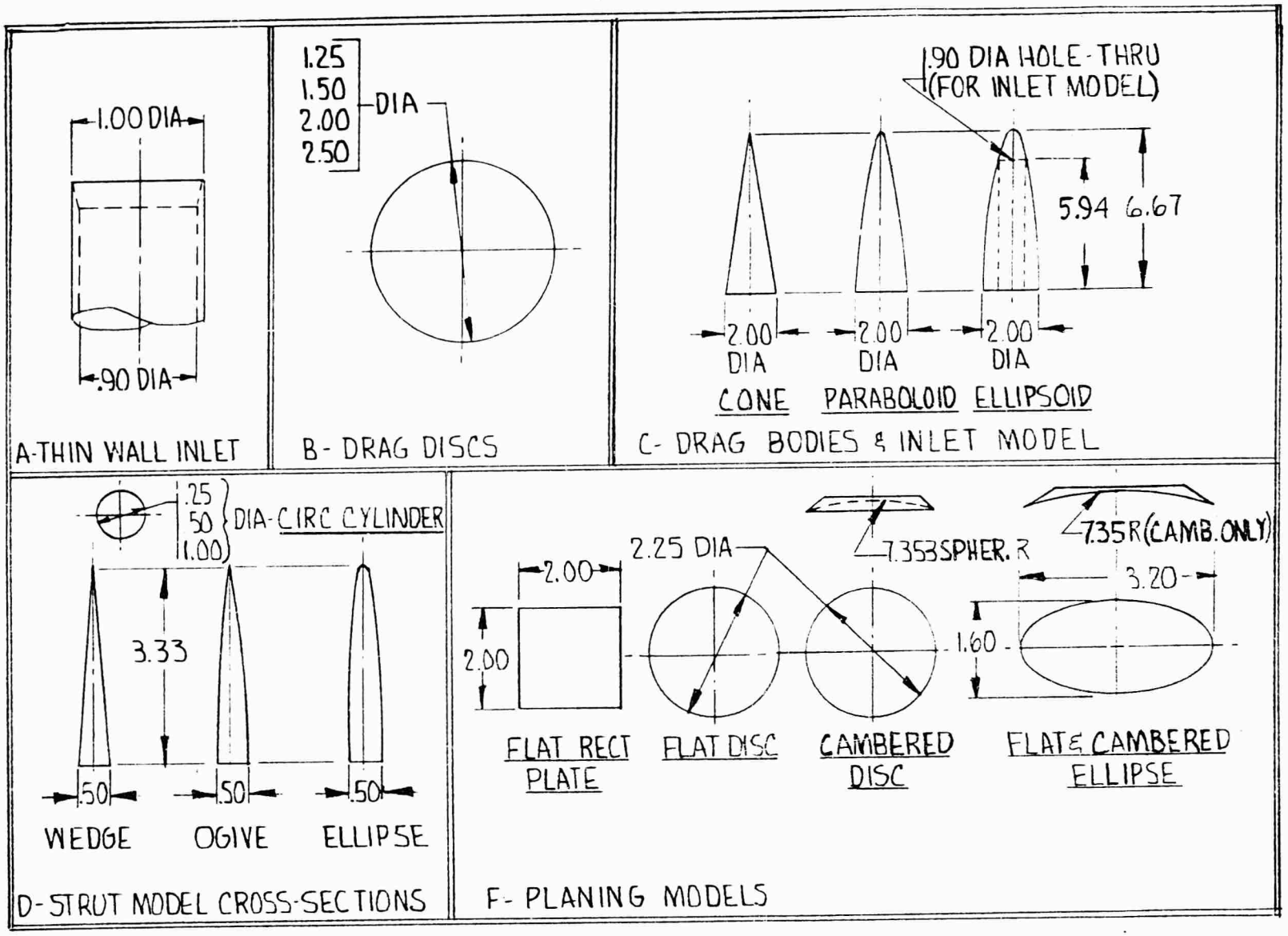

Figure 24. Model Geometry